2022

Multiple Shallow Crustal Origins for Spinel-bearing Lithologies on the Moon: A Perspective from the Luna 20 Mission

Steven B. Simon
sbs8@unm.edu

Charles K. Shearer
cshearer@unm.edu

Stephen E. Haggerty

Daniel P. Moriarty III

Noah Petro

See next page for additional authors

Multiple Shallow Crustal Origins for Spinel-Bearing Lithologies on the Moon: A Perspective from the Luna 20 Mission

S.B. Simon[1,2,3], C.K. Shearer[1,2,4], S.E. Haggerty[5], D. P. Moriarty III[6,7,8], N. Petro[6], J.J. Papike[1,2], and Z. Vaci[1,2]

[1]Institute of Meteoritics, University of New Mexico, Albuquerque, New Mexico 87131
[2]Department of Earth and Planetary Sciences, University of New Mexico, Albuquerque, New Mexico 87131
[3]Field Museum of Natural History, Chicago, Illinois
[4] Lunar and Planetary Institute, Houston, Texas
[5] Florida International University, Miami, Florida
[6]Goddard Space Flight Center, Greenbelt Maryland
[7]University of Maryland, College Park, Maryland
[8]Center for Research and Exploration in Space Science and Technology, University of Maryland, College Park, Maryland

Corresponding author: Steven Simon (sbs8@unm.edu)

Submitted to
Journal of Geophysical Research: Planets

February 2022
Revised August 2022

Key points:

Spinel-bearing lithic fragments found in the Luna 20 regolith provide insights into the origin and distribution of spinel-bearing lithologies on the Moon

Evidence for rapid cooling suggests these lithologies did not have deep sources and probably formed at relatively shallow depths

ABSTRACT

The Luna 20 mission returned samples from the Hilly and Furrowed Terrain of the Moon that is associated with the impact event that formed the Crisium Basin. This event potentially excavated deep crustal and upper mantle lithologies. Spinel is commonly considered to be a mineralogical indicator of rocks of high-pressure origin, and orbital data indicate the presence of spinel-bearing lithologies exterior to the basin. We have examined 166 Luna 20 particles in the 250-500 μm size range and found 31 spinel-bearing fragments. Of these 10 are igneous plutonic Mg-suite rocks, most of which are troctolitic, and 16 are impact melt rocks. The other five are fused soil or devitrified glass fragments. The spinel-bearing lithic fragments are plagioclase-rich and do not have the high modal abundances of Mg-Al spinel previously identified in the region through remote sensing analyses. The textures, compositions, and inferred crystallization sequences of the present magmatic spinel-bearing samples are most consistent with a relatively shallow crustal (rather than a deep crustal) origin, with a petrogenesis involving assimilation of ferroan anorthosite crust by Mg-rich, mantle-derived magmas. Both relict and newly-formed spinels are found in impact melt rocks and are also inferred to have formed at relatively low pressures. Thus, the presence of spinel is not an unambiguous indicator of mantle or deep crustal material. The insights gained from this study show that studies of a small, robotically collected sample can improve our understanding of regional lithologies and petrologic processes.

Plain Language Summary

Lunar rocks that contain spinel have long been thought to have formed at high pressures and have deep sources. A survey of lithic fragments in the Luna 20 regolith shows that spinel occurs in igneous and impact melt rocks with features more consistent with relatively rapid cooling than with slow cooling, and therefore relatively shallow depths of origin. The presence of spinel in a lunar rock is not an unambiguous indicator of mantle or deep crustal material.

1. INTRODUCTION

Spinel (predominantly the $MgAl_2O_4$-end member)-bearing crustal lithologies have long been recognized in the Apollo sample collection. However, such lithologies are rather rare and individual samples are small in mass (< 1 g). It has been inferred since the early 1970s that these lithologies (e.g., extensively shocked spinel ± cordierite troctolite clasts) were excavated during basin-forming events from the deep lunar crust and/or upper mantle (Anderson, 1973; Herzberg, 1978; Baker & Herzberg, 1980; Herzberg & Baker, 1980; Marvin et al., 1989; Snyder et al., 1998, 1999; Pieters et al., 2014). In addition, studies of lunar meteorites have revealed a unique lithology with high abundances of spinel (~30%) and an apparent shallow crustal origin (e.g., Gross & Treiman, 2011).

Another spinel-bearing lunar rock type, rich in Mg-Al spinel and plagioclase with limited Mg-rich olivine and pyroxene, was identified with near-infrared reflectance spectroscopy by the Moon Mineralogy Mapper instrument (M^3) during the Chandrayaan-1 mission (Pieters et al., 2009). At least 23 regions containing exposures of this lithology, termed pink-spinel anorthosite, were identified by Pieters et al. (2014). The spatial extent of each outcrop is on the order of ~100s of meters, and they are primarily distributed within regions of relatively thin crust. Sun et al. (2017) found the presence of Mg-spinel indicated in reflectance spectra for 38 of 166 central crater peaks that they analyzed, but only five of these appeared to also contain crystalline plagioclase.

Several pink-spinel anorthosite locations, represented in green in Fig. 1, are in the highland terrain surrounding the Crisium basin. In particular, the spinel location associated with Macrobius crater (lat 21.3°, long 46.1°) is within the noritic Hilly and Furrowed Terrain (Sliz & Spudis, 2016). Sliz and Spudis (2016) placed this Terrain into the Crisium Group and concluded that all units are Nectarian in age. Gravity data for the Crisium basin derived from the GRAIL mission show a very thin crust and suggest the possibility that the Crisium basin-forming event excavated lunar mantle (e.g., Wieczorek et al. 2013; Miljkovic et al., 2015; Neumann et al., 2015). Olivine along the rim of Crisium and the presence of this type of spinel-bearing lithology have been interpreted as representing material from the upper mantle and deep lunar crust (e.g., Yamamoto et al., 2010). The

interpretation of these lithologies still is a point of debate (e.g., Corley et al., 2018; Lemelin et al., 2019), however, and the presence of a monomineralic rock composed of olivine in the upper mantle may

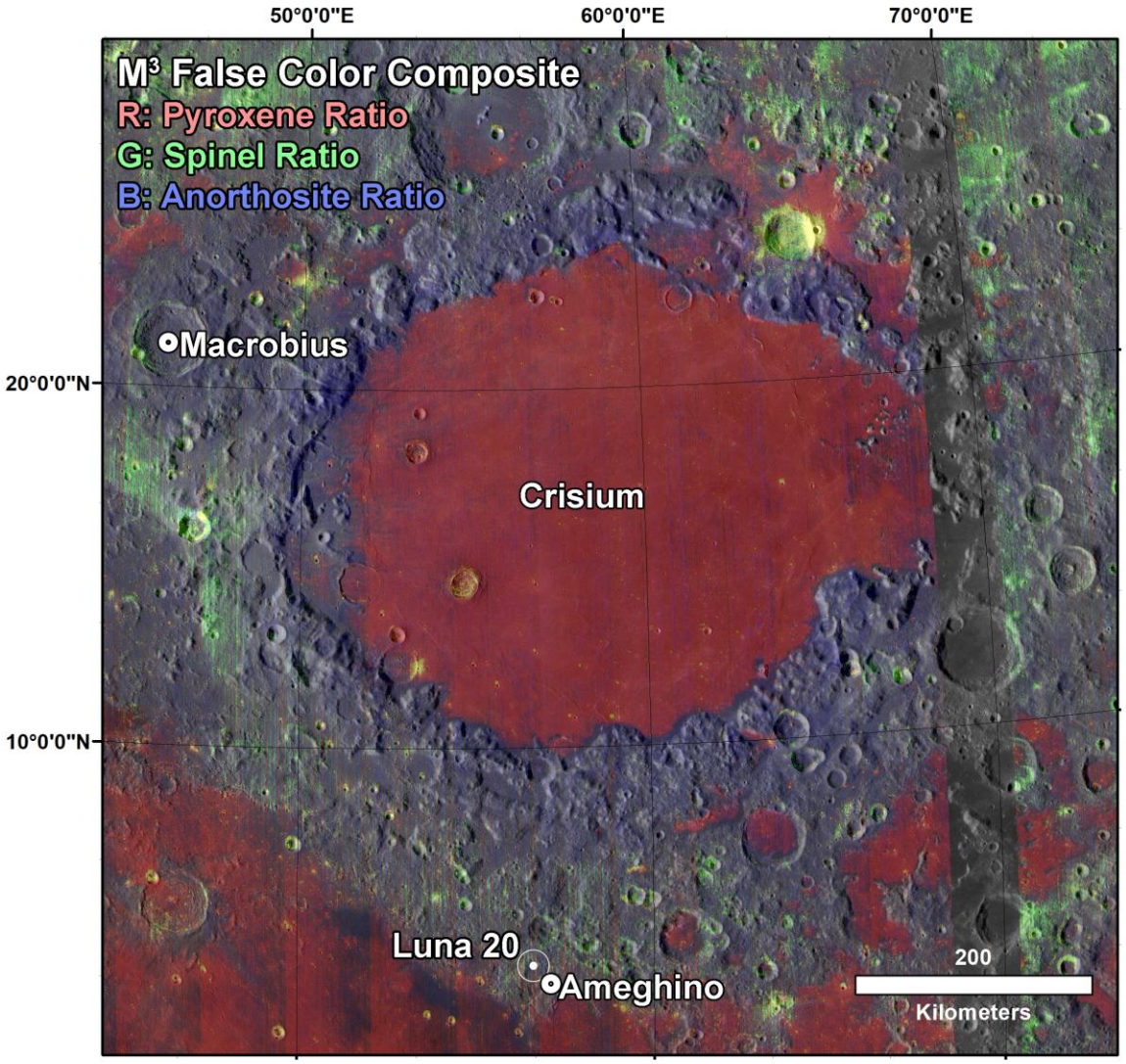

Figure 1. Moon Mineralogy Mapper (M^3) false color composite for the Crisium region, illustrating the geospatial distribution of spectral signatures associated with pyroxene (pink), spinel (green), and anorthosite (blue). The Luna 20 site and the nearby Ameghino crater exhibit spectral characteristics similar to those of the wider Hilly and Furrowed Terrain (HFT) surrounding Crisium Basin, suggesting that Luna 20 samples are representative of this region. Stark mineralogical differences are observed between the

HFT, the inner ring of Crisium, and mare basalts across the region. The parameters chosen here are described in full detail by Pieters et al (2014) and Moriarty et al. (2022).

not be consistent with dynamical models of mantle evolution (e.g., Boukaré et al., 2018; Moriarty et al., 2021a,b).

The Russian Luna 20 mission returned samples in 1972 from the noritic Hilly and Furrowed Terrain (Sliz & Spudis, 2016) approximately 200 km south of the inner ring of the Crisium basin (Lemelin et al., 2019). The sampling site is 33 km north of the edge of Mare Fecunditatis. The Luna 20 site is likely to be within Crisium's ejecta blanket, and therefore these samples may contain clues to the depth of material excavated during formation of the basin. The material at the Luna 20 site may also be partially derived from the 9 km Ameghino crater (Shearer et al., 2021), which is 15 km to the southeast of the landing site (Fig. 1) and is likely to have redistributed some amount of Crisium ejecta. Here, we examine crystalline spinel-bearing lithologies returned by the Luna 20 mission and consider them in the context of existing and new orbital observations.

There are four primary hypotheses for the petrogenesis of spinel-bearing lithologies on the Moon: (1) as cumulates or restites formed from basaltic systems at high pressure (Prinz et al., 1973; Anderson, 1973; Bence et al., 1974; Baker and Herzberg, 1980; Marvin et al., 1989; Snyder et al., 1998; Cohen et al., 2001; Takeda et al., 2006); (2) from troctolitic melts at low pressure (Walker et al., 1973; Marvin and Walker, 1985); (3) through hybridization of a mantle source or mantle-derived magma (assimilation or cumulate mixing) (Morgan et al., 2006; Gross & Treiman, 2011; Prissel et al., 2014; Shearer et al., 2015; Elardo et al., 2017, 2020); and (4) an exogenic origin, either through addition of a meteoritic component or due to an impact event (Pieters et al., 2011).

There are numerous spinel-bearing lithologies within the Luna 20 sample suite. Although these lithologies are distinct from those Mg-Al-spinel lithologies observed from orbit (e.g., Pieters et al., 2014) and those discovered within lunar meteorites (Gross & Treiman, 2011) with regard to modal abundances of spinel, they do have several similar characteristics, including being plagioclase-rich. Furthermore, they appear to have been derived through a variety of processes, and they provide important context concerning the origin of diverse spinel-bearing rocks. Here, we examine those lithologies and compare the

147 mineral assemblages and spinel chemistries with those of other lunar samples (Apollo
148 samples and meteorites). Using these data, we evaluate whether crystallization of spinel
149 occurred near the crust-mantle boundary or in shallow locations within the crust. We also
150 further explore petrogenetic models for the origin of lunar spinel-bearing lithologies
151 (magmas derived from the deep mantle, hybridization of sources, assimilation of ferroan
152 anorthosite crust by mantle derived magmas, or impact melting of crust) in the Crisium
153 region in particular and the Moon in general. Preliminary results were reported by Simon
154 et al. (2021; 2022).
155
156 ## 2. ANALYTICAL METHODS
157
158 Soon after their return, Luna 20 samples were shared with NASA as part of a United
159 States-Soviet Union sample exchange. Two mineralogy-petrology consortia were formed:
160 the "East-Coast Consortium" and the "Hinterland Consortium". These groups produced a
161 series of polished sections from different size fractions of these samples.
162 Polished thin sections of material sieved into the 250-500 μm size fraction (parent
163 split is 22003) and originally allocated to these consortia were acquired for this study.
164 Additional sections of 250-500 μm fragments allocated to NASA were also studied.
165 Sections were carbon-coated and examined with a TESCAN LYRA3 scanning electron
166 microscope (SEM) operated at 15kV. Quantitative energy-dispersive analyses (EDS) and
167 elemental X-ray maps were obtained with an IXRF silicon drift energy-dispersive X-ray
168 detector running Iridium Ultra software. Quantitative wavelength-dispersive analyses were
169 obtained with a fully automated JEOL 8200 electron microprobe operated at 15kV with a
170 focused beam, a beam current of 20 nA, calibrated with pure oxide and natural mineral
171 standards. Count times were 20s or 30s on peaks, 10s or 20s for background measurements,
172 respectively. Most detection limits are between 0.01 and 0.02 elemental wt%. Spinel
173 analyses were plotted on the modified Johnston prism using the Spinel Web software of
174 Antonini et al. (2020). The modal mineralogy of each fragment was determined by point-
175 counting 750–1200 points on backscattered electron images of the fragments, after
176 identification of the phases by X-ray mapping and EDS and WDS techniques.
177

178 # 3. RESULTS
179
180 Thirteen polished thin sections containing a total of 166 particles were examined
181 with the SEM. Most of these particles are lithic fragments, but monomineralic (mostly
182 plagioclase), fused soil (agglutinates and regolith breccias), and glass particles are also
183 present. Of the 166 particles, 31 contain spinel. Of these, 10 are crystalline magmatic rocks,
184 16 are impact melt rocks (e.g., impact melt breccias, including two fragments found in
185 agglutinates), and the other 5 are fused soil or devitrified glass fragments. The spinel-
186 bearing lithic fragments are plagioclase-rich but not modally spinel-rich, which is typical
187 of spinel-bearing lithologies found among the Apollo samples (e.g., Gross & Treiman,
188 2011). None of these Luna 20 spinel-bearing lithologies have the high modal abundance of
189 Mg-Al spinel (approximately 30%) of either the "pink-spinel" lithologies predicted from
190 orbital data (Dhingra et al., 2011; Pieters et al., 2014; Prissel et al., 2014) or found in the
191 unique lunar meteorite ALHA 81005 documented by Gross and Treiman (2011). Instead,
192 these lithologies more typically exhibit ~5% modal abundances of Fe-, Cr-bearing spinels.
193
194 ## 3.1. Petrography of Spinel-bearing Lithic Fragments
195
196 As noted above, the spinel-bearing lithic fragments consist of a variety of rock types
197 ranging from magmatic to impact in origin. The igneous rocks from Luna 20 were
198 originally classified as members of the highland plutonic anorthosite-norite-troctolite
199 (ANT) suite (e.g., G. Taylor et al., 1973; Bence & Grove, 1978). Within the context of
200 more recent terminology, these fragments fit within the Magnesian-suite (Mg-suite) or the
201 Ferroan Anorthosite suite (FANs). With one exception, the spinel-bearing plutonic rocks
202 examined in this study belong to the Mg-suite, based on their plagioclase compositions and
203 Mg#s (Mg/(Mg+Fe)) of mafic silicates (Shearer et al., 2021, 2022). They have mafic
204 mineral compositions that are too magnesian to plot with the ferroan anorthosites and their
205 plagioclase compositions are more calcic than those of alkali-suite lithologies (Shearer et
206 al., 2021, 2022).
207 For further classification, modal abundances of individual mineral phases were
208 determined from BSE images while recognizing that, as these are small fragments of

relatively coarse-grained, much larger units, any given fragment may not be representative of the bulk composition of its parent. Following the traditional terminology previously applied to these samples (e.g., Stöffler et al., 1980) and to feldspar-rich rocks in general, samples with ≥90% feldspar are anorthosites; those with 78-90% plagioclase are troctolitic, noritic, or gabbroic anorthosites depending on whether the dominant mafic phase is olivine, orthopyroxene, or clinopyroxene, respectively. With 60-78% plagioclase the rock is an anorthositic troctolite, norite, or gabbro, and with 10-60% plagioclase, simply a troctolite, norite, gabbro, or olivine-norite/gabbro. Modal mineralogies of Luna 20 spinel-bearing lithologies are compared to those of other lithologies present at the site, and to those associated with the inner rim of the Crisium Basin, by Shearer et al. (2021, 2022). In the sample suite considered here, the most common spinel-bearing igneous rock type is spinel troctolite, followed by anorthositic troctolite, gabbroic anorthosite, high-alumina basalt, and troctolitic anorthosite (Table 1).

Table 1

Representative Compositions of Silicates in Spinel-bearing Igneous Lithic Fragments in the 250–500 μm Fraction of Luna 20 Soil 22003

Section	Fragment #	Rock type	Mole % An	Mole % Fo	Pyx EnWoFs
,6	5	High-Al Bas.	95.5	86.0	$E_{48.1}W_{43.9}F_{8.0}$
,10	1	Anorthc. Troct.	93.9	82.4	$E_{82.6}W_{3.1}F_{14.3}$
,22	16	Troctc. Anorth.	95.1	85.1	$E_{41.8}W_{43.8}F_{14.4}$
,31	10	Spinel Troct.	93.9	83.6	
,31	11	Spinel Troct.	95.1	84.4	$E_{59.1}W_{37.4}F_{3.5}$
,31	15	Spinel Troct.	94.7	84.1	
,9005	7	Gabbroic An.	95.4	88.0	$E_{56.7}W_{33.1}F_{10.2}$
,9010	16	Anorthc. Troct.	94.3	85.7	$E_{85.4}W_{7.4}F_{7.2}$
,9014	4	Gabbroic An.	95.2		$E_{45.5}W_{17.9}F_{36.6}$
,9014	12	Spinel Troct.	95.0	83.7, 90.4	$E_{42.0}W_{43.4}F_{14.6}$

Abbreviations: Bas.: basalt; Anorthc.: anorthositic; Anorth., An.: anorthosite; Troctc: troctolitic; Troct.: troctolite; An: anorthite; Fo: forsterite; Pyx: pyroxene; En: enstatite; Wo: wollastonite; Fs: ferrosilite.

Backscattered electron images of representative spinel-bearing igneous rock fragments from Luna 20 are shown in Fig. 2. The samples shown are an anorthositic troctolite (Fig. 2a), a gabbroic anorthosite (Fig. 2b), and two spinel troctolites (Fig. 2c,d).

234 The anorthositic troctolite has coarse plagioclase, olivine, and pyroxene, and fine FeS and
235 Cr-rich spinel. The gabbroic anorthosite also has plagioclase, more pyroxene than olivine,
236 and Mg-Al spinel. One of the spinel troctolites (Fig. 2c) has subequal proportions of
237 plagioclase and olivine and both Cr-rich spinel and Mg-Al spinel. The other spinel
238 troctolite (Fig. 2d) is more plagioclase-rich, has Mg-Al spinel, minor clinopyroxene, very
239 magnesian olivine (Fo_{96}) and less forsteritic olivine (Fo_{92}). Grains of the latter are embayed,
240 suggesting that they were not in equilibrium with the olivine-plagioclase assemblage. The
241 interpretation and importance of this texture is considered below in the Discussion.
242 Backscattered electron images of representative spinel-bearing impact melt rocks
243 are shown in Fig. 3. Impact melt rocks are common in lunar regoliths with large highland
244 components. The spinel-bearing ones in the present suite typically have relatively coarse
245 plagioclase clasts and relict-looking Mg-Al spinel grains in a finer (10–20 μm) matrix of
246 plagioclase, pyroxene, and olivine. The fine textures of the matrices indicate rapid cooling,
247 and they are generally composed of plagioclase laths with interstitial olivine ± pyroxene.
248 Olivine is much more abundant than pyroxene in these rocks. G. Taylor et al. (1973) also
249 noted that in many Luna 20 lithic fragments, olivine is the dominant or even the only mafic
250 silicate, especially in spinel-bearing fragments.
251 An unusual spinel occurrence is shown in Fig. 4. A small grain of Cr-rich spinel is
252 enclosed in nearly pure Mg-Al spinel in an impact melt breccia. Plagioclase laths radiate
253 outward from a large, probably relict, olivine grain (Fig. 4b). The sample appears to contain
254 multiple generations of olivine and spinel. The overgrowth of Mg-Al spinel on Cr-rich
255 spinel is shown in Fig. 4c. Also shown is an adjacent region of finely intergrown
256 plagioclase and pyroxene plus euhedral olivine.
257

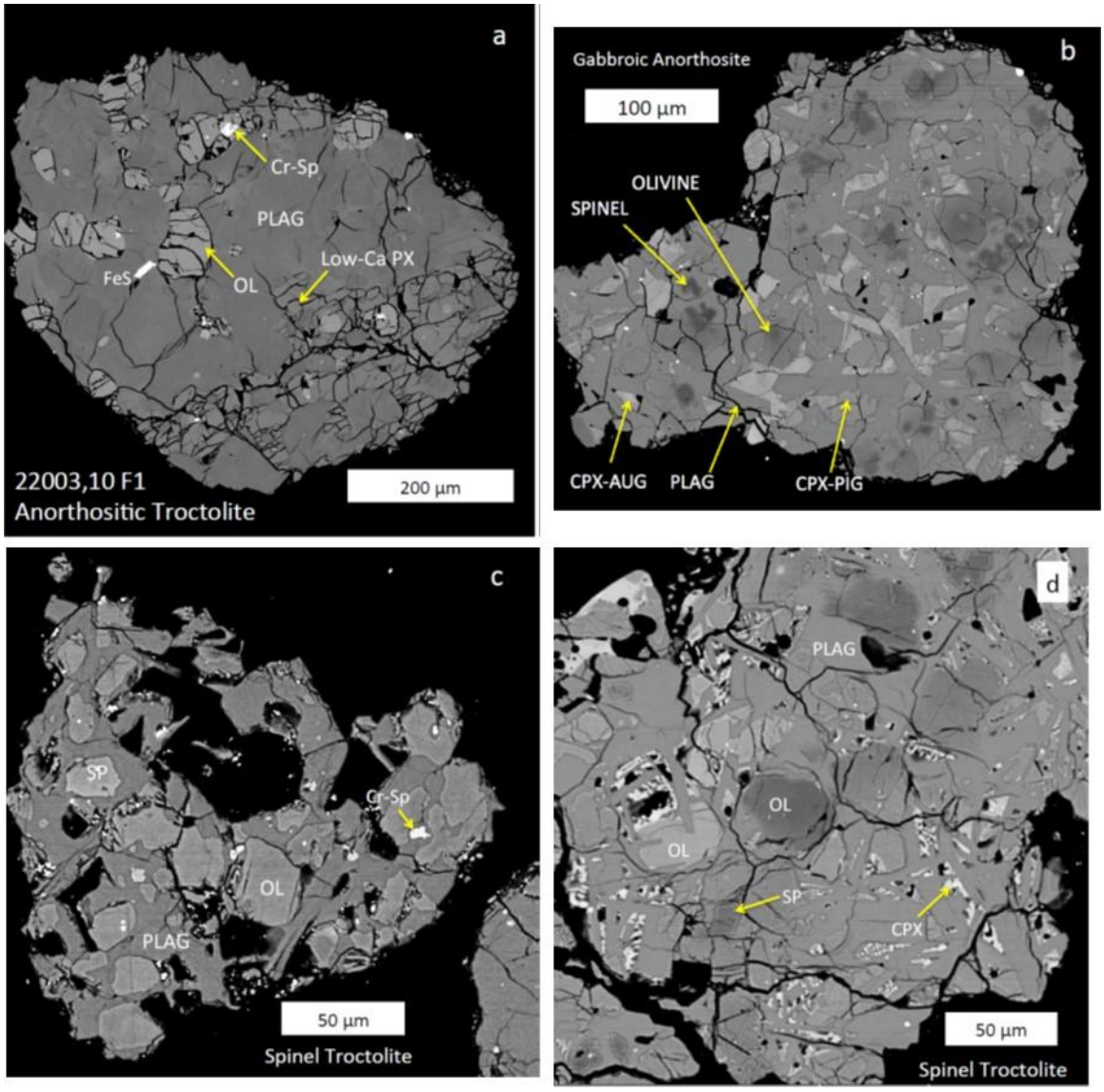

Figure 2. Backscattered electron images of spinel-bearing igneous lithic fragments. (a) 22003,10 fragment 1, an anorthositic troctolite with anhedral olivine, low-Ca pyroxene and Cr-rich spinel. (b) 22003,9005 fragment 7, a gabbroic anorthosite with high-Ca and low-Ca pyroxene, minor olivine and Mg-, Al spinel. (c) 22003,31 fragment 10, a spinel troctolite with relatively coarse olivine and spinel. (d) 22003,9014 fragment 12, a spinel troctolite with both very forsteritic (Fo_{96}, dark) and less forsteritic (Fo_{92}, light) olivine with fine Ca-rich pyroxene interstitial to plagioclase. PLAG: plagioclase; CPX: clinopyroxene; OL: olivine; SP: spinel; AUG: augite; PIG: pigeonite.

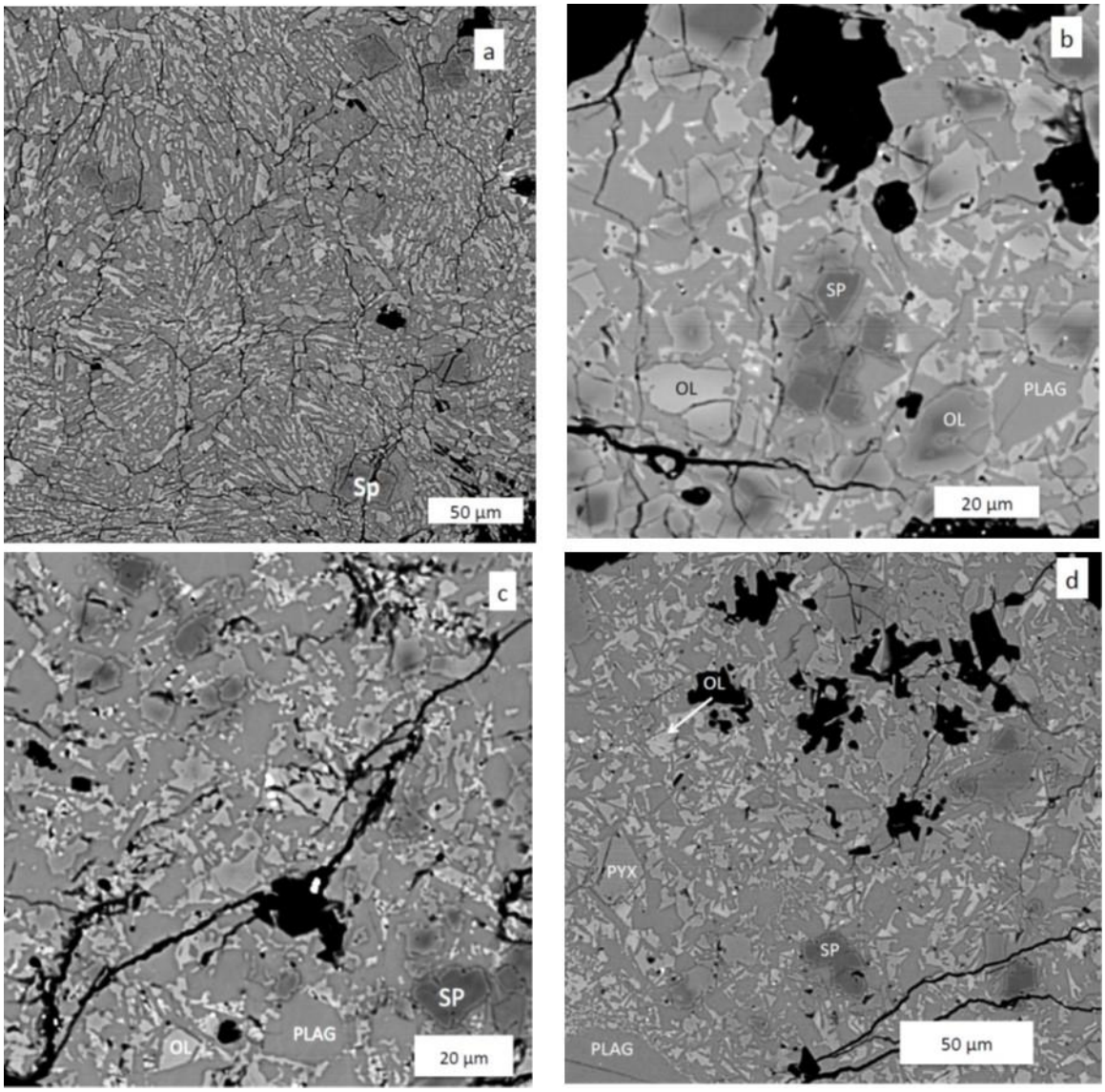

Figure 3. Backscattered electron images of spinel-bearing impact melt rocks. (a) 22003,6 Fragment 16. Fine, blebby olivine and clinopyroxene (light) with Mg-Al spinel (Sp, dark) and fine plagioclase (dark gray). (b) 22003,22 Fragment 7. Melt rock with coarse olivine clasts in a matrix of fine plagioclase laths and interstitial olivine. Most coarse olivine clasts have forsteritic cores and are more magnesian than interstitial olivine. The forsteritic cores and Mg-Al spinels may be relict grains from the target rock. (c) 22003,30 Fragment 2, a poikilitic, feldspar-rich crystalline melt breccia with Mg-Al spinel and minor Fe metal. (d) 22003,9010 F14. Crystalline melt breccia with clasts of plagioclase and spinel in a matrix of plagioclase laths with interstitial olivine and pyroxene. Abbreviations as in Fig. 2.

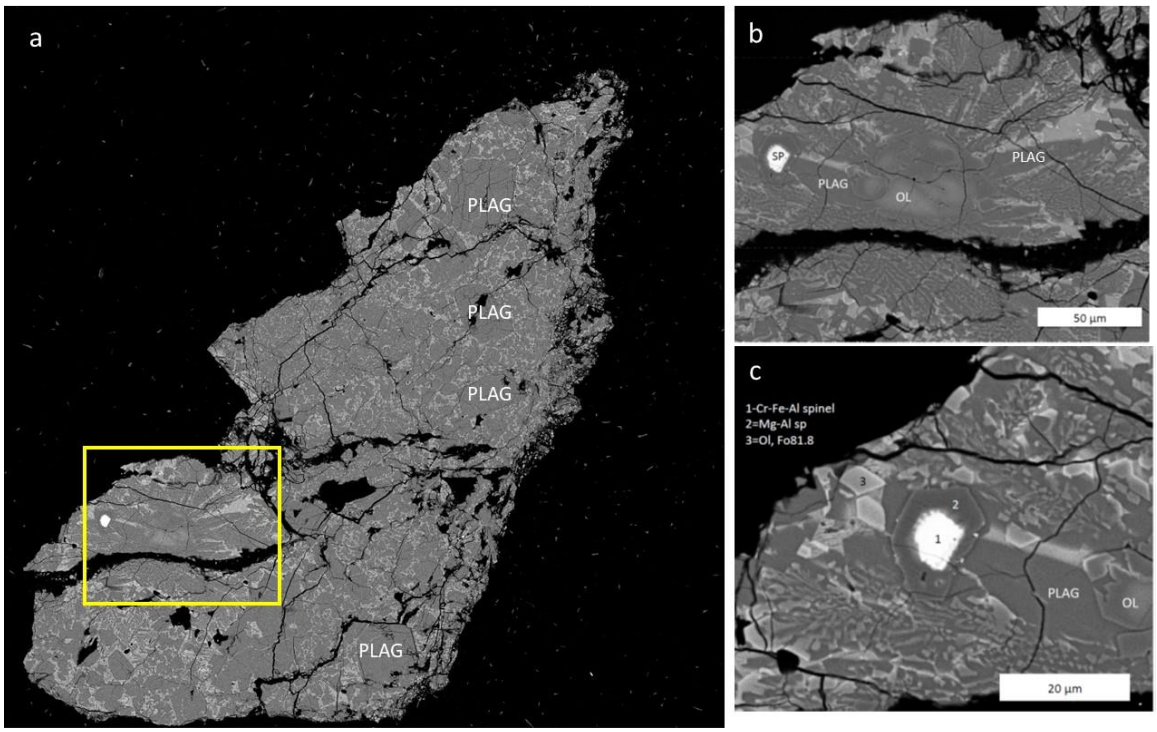

Figure 4. Impact melt breccia 22003,6 fragment 3. (a) Image of complete fragment illustrating that plagioclase was the dominant component making up the unmelted portion (clasts) of the breccia. Pre-melting mineral assemblage was most likely plagioclase + olivine + Cr-Fe spinel. The field of image (b) is indicated by the box. (b) Cr-Fe spinel (SP) enclosed in Mg-Al spinel, and relatively Fe-rich olivine (OL) enclosed in more forsteritic olivine. Plagioclase laths appear to have nucleated on the olivine and radiate away from it. (c) Higher-magnification view of spinel grain shown in (a) and (b). Note subhedral Mg-Al spinel (2) enclosing Cr-Fe-Al spinel (1), small olivine grains (3), and the fine intergrowth of pyroxene and plagioclase below the spinel.

3.2. Mineral Chemistry

3.2.1. Silicates

Compositions of feldspar, pyroxene, and olivine in spinel-bearing igneous lithic fragments are summarized in Table 1. No exsolution lamellae were observed in pyroxene in spinel-bearing samples at the scale of greater than 1 micron in width. This is not surprising, as pyroxene in lithologies from the Luna 20 site exhibits complex and fine

exsolution lamellae on the scale of 10Å to 1-3μm (Prinz et al., 1973; Meyer, 1973; Ghose et al., 1973; Shearer et al., 2021). Except for two gabbroic anorthosites and one high-alumina basalt, the present samples have olivine as the dominant mafic silicate (i.e., they are classified as troctolites or troctolitic). Plagioclase in spinel-bearing lithics, as in most highland rocks, is very calcic, with compositions mostly between 93 and 96 mole % anorthite. Prinz et al. (1973) and Cameron et al. (1973) also found most plagioclase in Luna 20 igneous lithic fragments to be more calcic than An_{90}, and Cameron et al. (1973) observed that to be the case for breccias and single crystals of plagioclase as well.

As is typical of troctolitic lithologies, olivine in the present samples is Mg-rich, with compositions more magnesian than Fo_{80} and within the previously reported range. Prinz et al. (1973) showed that olivine in Luna 20 troctolites is more magnesian (mostly $Fo_{80–90}$) than that in the other highland lithologies at L-20, which are mostly between Fo_{60} and Fo_{80}.

Pyroxene was not found in all samples listed in Table 1, but where present, in most cases it has high Mg/(Mg+Fe) and low TiO_2 contents (≤~1 wt%). Representative electron probe analyses of pyroxene in Luna 20 igneous spinel-bearing lithic fragments are given in Table 2. Prinz et al. (1973) found only Mg-rich, Ca-poor (≤10 mole % wollastonite component) pyroxene in Luna 20 troctolite but much wider ranges of both Mg and Ca contents in their "noritic and troctolitic anorthosite" and "anorthositic norite and troctolite" groups. Among the present samples, of the five troctolitic samples that have pyroxene, three have high-Ca pyroxene ($Wo_{>37}$) and two have low-Ca pyroxene ($Wo_{<8}$).

320

321 **Table 2**

322 *Representative electron probe analyses of pyroxene in igneous Luna 20 lithic fragments.*

	1.	**2.**	**3.**	**4.**	**5.**	**6.**	**7.** 323
	AB	**AT**	**AT**	**GA**	**GA**	**GA**	**GA**
Na_2O	0.04	0.09	0.00	0.21	0.11	0.11	0.08
MgO	16.44	17.31	29.83	15.13	15.51	14.89	15.46
Al_2O_3	4.29	1.57	0.96	2.60	0.80	1.32	0.83
SiO_2	52.07	52.54	55.22	50.86	51.93	51.47	51.28
CaO	20.87	22.66	1.72	6.02	8.52	10.93	8.31
TiO_2	1.10	0.89	0.46	0.35	0.39	0.41	0.46
V_2O_3	0.10	0.10	0.02	0.04	0.05	0.02	0.00
Cr_2O_3	0.44	0.87	0.52	0.17	0.27	0.27	0.28
MnO	0.13	0.10	0.18	0.42	0.35	0.33	0.40
FeO	4.85	4.14	10.45	23.95	22.25	20.59	23.12
Total	100.34	100.26	99.37	99.74	100.19	100.35	100.22
				Cations per 6 oxygen anions			
Na	0.003	0.006	0.000	0.015	0.008	0.008	0.006
Mg	0.890	0.943	1.581	0.863	0.881	0.844	0.882
Al	0.184	0.068	0.040	0.117	0.036	0.059	0.037
Si	1.892	1.921	1.964	1.947	1.978	1.959	1.964
Ca	0.812	0.888	0.066	0.247	0.348	0.446	0.341
Ti	0.030	0.024	0.012	0.010	0.011	0.012	0.013
V	0.003	0.003	0.001	0.001	0.002	0.001	0.000
Cr	0.013	0.025	0.015	0.005	0.008	0.008	0.009
Mn	0.004	0.003	0.005	0.014	0.011	0.011	0.013
Fe	0.147	0.127	0.311	0.767	0.709	0.655	0.741
Total	3.979	4.008	3.996	3.987	3.991	4.003	4.006
En	48.13	48.19	80.76	46.00	45.46	43.40	44.92
Wo	43.91	45.35	3.35	13.15	17.95	22.91	17.37
Fs	7.96	6.46	15.88	40.85	36.58	33.69	37.71

324 Parent of all samples is 22003. Analysis 1.: ,6 Fragment 5. 2., 3.: ,10 Fragment 1.
325 4. - 7.: ,9014 Fragment 4. 8. - 12.: ,9005 Fragment 7. 13.: ,9014 Fragment 12. AB:
326 aluminous basalt. AT: anorthositic troctolite. GA: gabbroic anorthosite. SPT:
327 spinel troctolite.
328

329

Table 2 continued

	8. GA	9. GA	10. GA	11. GA	12. GA	13. SPT
Na_2O	0.04	0.02	0.03	0.06	0.03	0.26
MgO	18.41	23.77	20.81	20.32	19.94	13.80
Al_2O_3	4.09	1.56	3.42	4.92	3.24	3.57
SiO_2	52.73	54.24	53.78	53.67	52.24	52.31
CaO	18.41	9.05	14.52	15.44	16.19	19.85
TiO_2	0.74	0.60	0.58	0.78	0.60	1.45
V_2O_3	0.09	0.05	0.05	0.06	0.02	0.12
Cr_2O_3	0.42	0.14	0.43	0.24	0.36	0.49
MnO	0.12	0.15	0.12	0.10	0.15	0.22
FeO	5.09	10.12	6.27	5.59	6.36	8.58
Total	100.13	99.68	100.01	101.18	99.11	100.65
			Cations per 6 oxygen anions			
Na	0.003	0.001	0.002	0.004	0.002	0.019
Mg	0.992	1.280	1.114	1.074	1.087	0.756
Al	0.174	0.066	0.145	0.205	0.139	0.154
Si	1.906	1.959	1.932	1.903	1.911	1.922
Ca	0.713	0.350	0.559	0.586	0.634	0.782
Ti	0.020	0.016	0.016	0.021	0.016	0.040
V	0.002	0.002	0.001	0.002	0.001	0.004
Cr	0.012	0.004	0.012	0.007	0.010	0.014
Mn	0.004	0.004	0.004	0.003	0.005	0.007
Fe	0.154	0.306	0.188	0.166	0.195	0.264
Total	3.981	3.989	3.973	3.971	4.000	3.961
En	53.36	66.12	59.86	58.81	56.73	41.97
Wo	38.36	18.08	30.03	32.11	33.12	43.39
Fs	8.28	15.79	10.12	9.08	10.15	14.64

Compositions of silicate minerals in spinel-bearing impact melt breccias are summarized in Table 3. Plagioclase compositions have a wider range, An_{90-97}, than seen in the igneous samples, but they are still quite calcic. Plagioclase analyses in this compositional range were also reported by Cameron et al. (1973) for recrystallized polymict breccias, which are presumably analogous to our impact melt breccia group. Except for one sample, olivine is more magnesian than Fo_{80}, and most samples fall in the range of Fo_{80-90}. These samples contain more olivine than pyroxene. In four of the five samples that have fairly uniform compositions, the pyroxene is Mg-rich and Ca-poor. The

remaining sample, 22003,6 F16 has a range of compositions. The En range is 52-82 mole%, that of Wo is 5 to 41, and that of Fs is 7 to 13. The composition shown in Table 3 is an average of nine analyses, and it is similar to several of the individual analyses.

Table 3

Representative Compositions of Silicates in Spinel-bearing Impact Melt Breccia Fragments in the 250–500 µm Fraction of Luna 20 Soil 22003

Section	Fragment #	Mole % An	Mole % Fo	Pyx (EnWoFs)
,6	3	94.5	78.0*	$E_{63.6}W_{5.7}F_{30.7}$**
,6	12	94.6	91.7	
,6	16	96.6	85.2	$E_{66.4}W_{23.4}F_{10.2}$
,22	7	93.6	87.2	
,22	26	90.4	93.9	$E_{65.5}W_{9.6}F_{24.9}$
,30	2	93.6	86.0	
,30	9	93.2	82.0	
,30	10	94.4	83.6	
,31	12	92.3	88.0	
,9004	8	92.1		$E_{82.4}W_{5.4}F_{12.2}$
,9004	9	94.8	76.8	$E_{70.9}W_{11.7}F_{17.4}$
,9010	4	93.8	84.9	
,9010	9	93.8	83.2	
,9010	14	92.4	92.3	$E_{85.5}W_{4.2}F_{10.0}$
,9013	8	91.3	93.0	
,9014	18	93.6	89.8	

*Average of matrix (71.1) and relict (84.8) grain compositions.
**Average of nine analyses.
Abbreviations as in Table 1.

3.2.2. Spinel

The general structural formula for the spinel group is $^{IV}A^{VI}B_2O_4$, where the "^{IV}" and "^{VI}" refer to cations in tetrahedral and octahedral coordination, respectively. In the normal spinel structure, the divalent cations (Fe^{2+}, Mg) occupy only the tetrahedral (A) site and the two octahedral (B) sites contain higher-charged cations (e.g., Fe^{3+}, Cr^{3+}, Al^{3+}, Ti^{4+}). If the divalent cations occur in one half of the octahedral sites, the mineral is referred to as an inverse spinel. Both normal and inverse spinels occur on the Moon. Spinel compositions can generally be described as combinations of Mg-, Al-, Cr-, Ti-, and Fe^{2+}-rich components (e.g., $MgAl_2O_4$ = spinel (*sensu stricto*), $Fe^{2+}Cr_2O_4$ = chromite, $Fe^{2+}Fe^{2+}TiO_4$ = ulvöspinel,

362 $FeAl_2O_4$ = hercynite, $MgCr_2O_4$ = pichrochromite). As defined by Haggerty (1972),
363 terminology with respect to these endmembers and the associated compositional fields in
364 the modified Johnston prism are illustrated in Fig. 5. Nearly pure $MgAl_2O_4$, and grains
365 dominated by this component, with variable Cr and Fe contents, are common in the present
366 samples. As shown in Fig. 6a, spinel compositions in Luna 20 samples reported in 1973
367 consortia studies range from nearly pure $MgAl_2O_4$ through chromian pleonaste, Mg-Al
368 chromite, Al-Ti chromite, and chromian-ulvöspinel (see Fig. 5 for definitions). The present
369 samples (Fig. 6b) fall on a low-Ti fractionation trend, also seen by Haggerty (1973), from
370 spinel through chromian-pleonaste toward chromite. Representative analyses of spinel
371 found in plutonic rocks and impact melt breccias in the present study are given in Table 4
372 and Table 5, respectively, showing low contents of TiO_2 and other minor elements.
373

Table 4.
Representative electron probe analyses of spinel in igneous Luna 20 lithic fragments.

	1. AB	2. AT	3. TA	4. TA	5. GA	6. GA	7. GA	8. SPT	9. SPT	10. SPT	11. SPT	12. SPT	13. SPT	14. SPT
MgO	21.30	5.09	20.44	20.77	21.68	22.32	23.76	19.46	17.59	18.20	18.11	21.53	21.51	21.80
Al_2O_3	65.03	12.92	63.80	60.96	64.43	65.07	65.86	58.77	51.98	54.20	54.57	65.29	64.18	65.68
SiO_2	0.21	0.25	0.24	0.59	0.25	0.15	0.22	0.26	0.32	0.24	1.74	0.17	0.92	0.24
CaO	0.08	0.48	0.04	0.05	0.08	0.08	0.17	0.17	0.34	0.27	0.95	0.13	0.37	0.17
TiO_2	0.26	2.02	0.23	0.21	0.17	0.11	0.06	0.48	0.25	0.19	0.46	0.07	0.08	0.09
V_2O_3	0.06	0.50	0.15	0.22	0.04	0.04	0.05	0.11	0.16	0.11	0.10	0.04	0.05	0.04
Cr_2O_3	1.84	48.86	3.10	4.69	2.03	1.72	1.81	6.67	14.15	11.90	10.51	1.97	2.21	1.84
MnO	0.07	0.42	0.08	0.09	0.06	0.08	0.06	0.09	0.13	0.12	0.12	0.08	0.06	0.06
FeO	9.84	27.17	11.08	10.58	9.62	8.62	6.48	12.17	13.00	12.47	12.42	9.63	8.92	8.97
Total	98.69	97.71	99.15	98.16	98.36	98.26	98.46	98.19	97.92	97.71	98.98	98.92	98.31	98.89
	Cations per 4 oxygen anions													
Mg	0.803	0.261	0.775	0.799	0.820	0.841	0.884	0.760	0.711	0.729	0.711	0.809	0.811	0.816
Al	1.938	0.525	1.911	1.854	1.927	1.938	1.938	1.815	1.661	1.716	1.695	1.941	1.914	1.945
Si	0.005	0.009	0.006	0.015	0.006	0.004	0.005	0.007	0.009	0.007	0.046	0.005	0.023	0.006
Ca	0.002	0.018	0.001	0.001	0.002	0.002	0.005	0.005	0.010	0.008	0.027	0.004	0.010	0.005
Cr	0.037	1.331	0.062	0.096	0.041	0.034	0.036	0.138	0.303	0.253	0.219	0.039	0.044	0.037
Ti	0.005	0.052	0.004	0.004	0.003	0.002	0.001	0.009	0.005	0.004	0.009	0.001	0.002	0.002
V	0.001	0.015	0.003	0.004	0.001	0.001	0.001	0.002	0.004	0.002	0.002	0.001	0.001	0.001
Mn	0.001	0.012	0.002	0.002	0.001	0.002	0.001	0.002	0.003	0.003	0.003	0.002	0.001	0.001
Fe	0.208	0.783	0.236	0.228	0.204	0.182	0.135	0.267	0.295	0.280	0.274	0.203	0.189	0.188
Total	3.000	3.005	3.000	3.003	3.005	3.006	3.006	3.006	3.000	3.002	2.986	3.005	2.996	3.001

Parent of all samples is 22003. Analysis 1.: ,6 Fragment 5. 2.: ,10 Fragment 1. 3. and 4.: ,22 Fragment 16. 5.-7.: ,9005 Fragment 7. 8.: ,31 Fragment 10. 9. and 10.: ,31 Fragment 11. 11.: ,31 Fragment 15. 12.-14.: ,9014 Fragment 12. AB: aluminous basalt. AT: anorthositic troctolite. TA: troctolitic anorthosite. GA: gabbroic anorthosite. SPT: spinel troctolite.

374
375
376
377
378
379
380
381
382
383
384

Table 5

Representative electron probe analyses of spinel in Luna 20 impact melt breccias.

	1.	2.	3.	4.
MgO	20.83	20.33	7.73	22.28
Al_2O_3	65.88	65.21	10.30	65.96
SiO_2	0.06	0.11	0.06	0.16
CaO	0.06	0.08	0.124	0.06
Cr_2O_3	1.89	2.12	55.57	5.45
TiO_2	0.28	0.29	1.86	0.04
V_2O_3	0.04	0.06	0.50	0.03
MnO	0.09	0.09	0.31	0.06
FeO	11.02	10.67	22.86	7.57
Total	100.15	98.96	99.31	101.61
	Cations per 4 oxygen anions			
Mg	0.777	0.767	0.388	0.814
Al	1.945	1.947	0.409	1.906
Si	0.001	0.003	0.002	0.004
Ca	0.001	0.002	0.004	0.002
Cr	0.038	0.043	1.481	0.106
Ti	0.005	0.005	0.047	0.001
V	0.001	0.001	0.013	0.001
Mn	0.002	0.002	0.009	0.001
Fe	0.231	0.226	0.644	0.155
Total	3.001	2.996	2.997	2.990

1. and 2.: 22003,6 Fragment 16.
3. and 4.: 22003,6 Fragment 3.

398

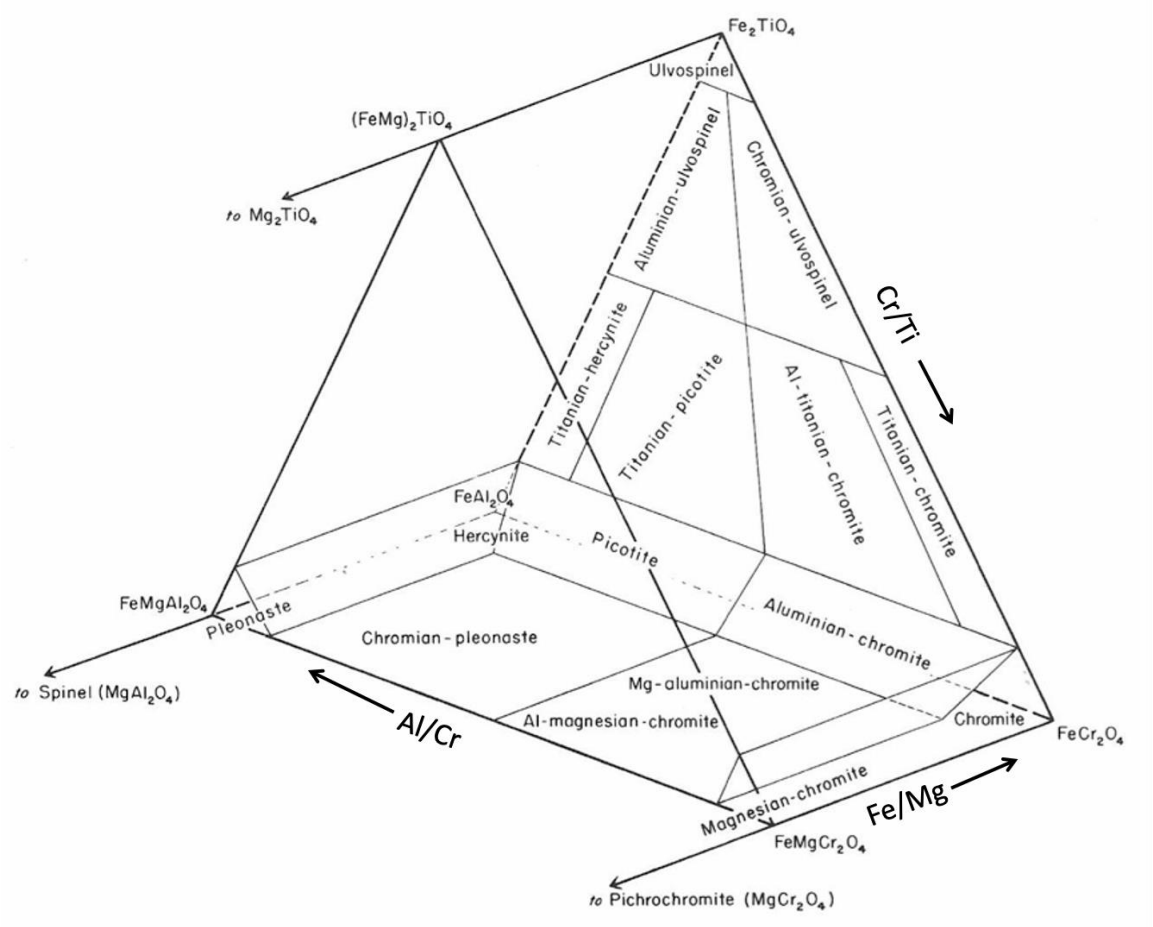

399

400 **Figure 5.** Spinel nomenclature for compositions with Fe/Mg ≥ 1 in the modified Johnston
401 prism. After Haggerty (1972).

402

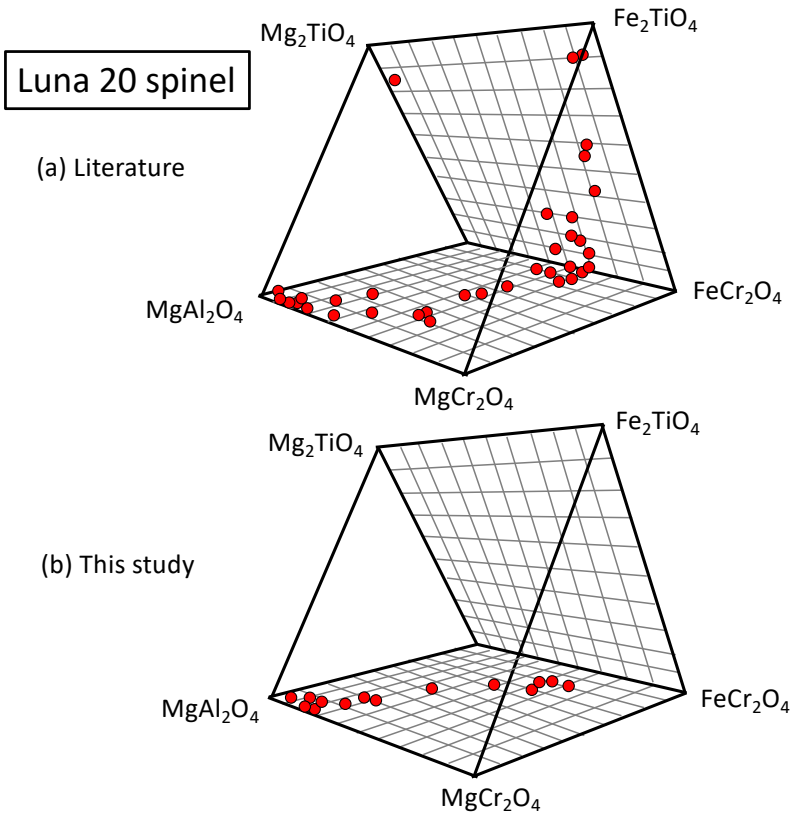

Figure 6. Compositions of Luna 20 spinels plotted on the modified Johnston prism. (a) Analyses are from the initial work on Luna 20 samples, and mostly from Brett et al. (1973). (b) Analyses from this study, in which a narrower range of rock types were investigated than in the compilation of studies represented in (a). Data were plotted with the software of Antonini et al. (2020).

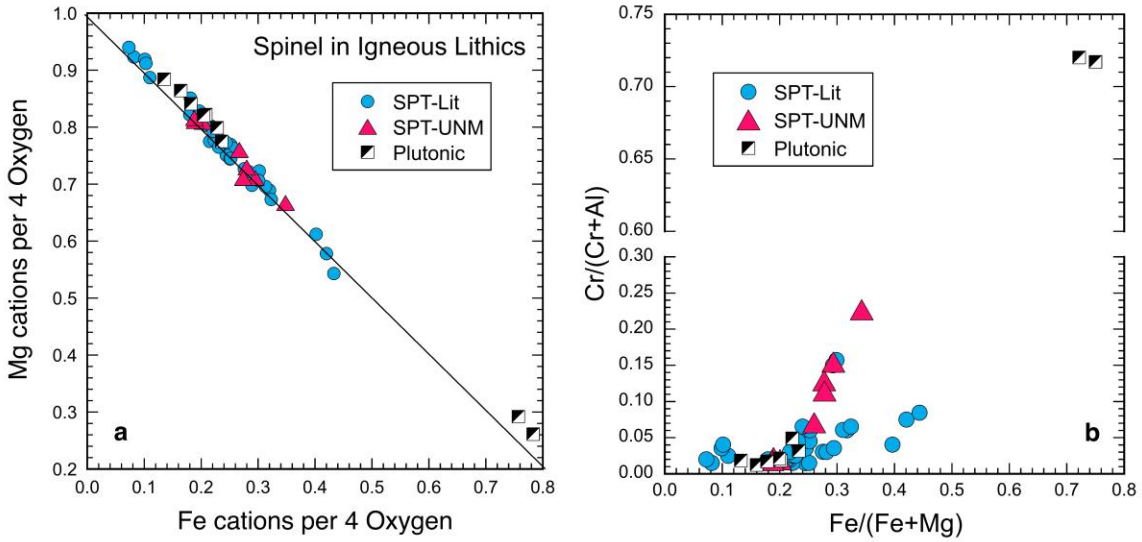

Figure 7. Compositions of spinel in Luna 20 igneous lithic fragments. (a) Mg vs. Fe cations per formula unit. Line of slope –1 is shown for reference. (b) Atomic Cr/(Cr +Al) vs. Fe/(Fe + Mg). SPT-Lit: analyses of spinel in spinel troctolites from Brett et al. (1973); SPT-UNM: analyses of spinel in spinel troctolite collected for this study; Plutonic: analyses of spinel in plutonic fragments other than spinel troctolite, collected for this study.

Some interelement relationships among the present Luna 20 spinels are illustrated in Fig. 7. The dominance of Fe-Mg substitution is shown by the strong anticorrelation between Fe and Mg seen in Fig. 7a, with the analyses plotting on or near the slope –1 line that is shown for reference. Most of the spinel in troctolitic lithologies (SPT) and in impact melt breccias has high Mg:Fe ratios, but Fe-, Cr-rich grains are also found. Both Mg-rich and Fe-rich spinel occurs in other plutonic rocks. The analyses reported by Brett et al. (1973) and plotted in Fig. 7 have a range of Cr_2O_3 contents for SPT spinel of 1.4 to 14.4 wt%, but, as shown in Fig. 7b, these grains have a limited range of Cr/(Cr + Al) ratios. Neither Brett et al. (1973) nor Prinz et al. (1973) found either chromite or ulvöspinel in the spinel troctolite samples they studied. The Cr-, Fe-rich grains we found are very small (Fig. 2), on the order of a few microns, and would be difficult to identify optically.

Analyses of spinel in Luna 20 impact melt breccias are plotted in Fig. 8. The Mg and Fe cation abundances plot on or slightly below the slope –1 reference line (Fig. 8a). As Fig. 8b shows, they have lower Cr/(Cr+Al) ratios than most of the spinel in the spinel troctolites (Fig. 7b) but similar to spinel in the other plutonics. Representative analyses are

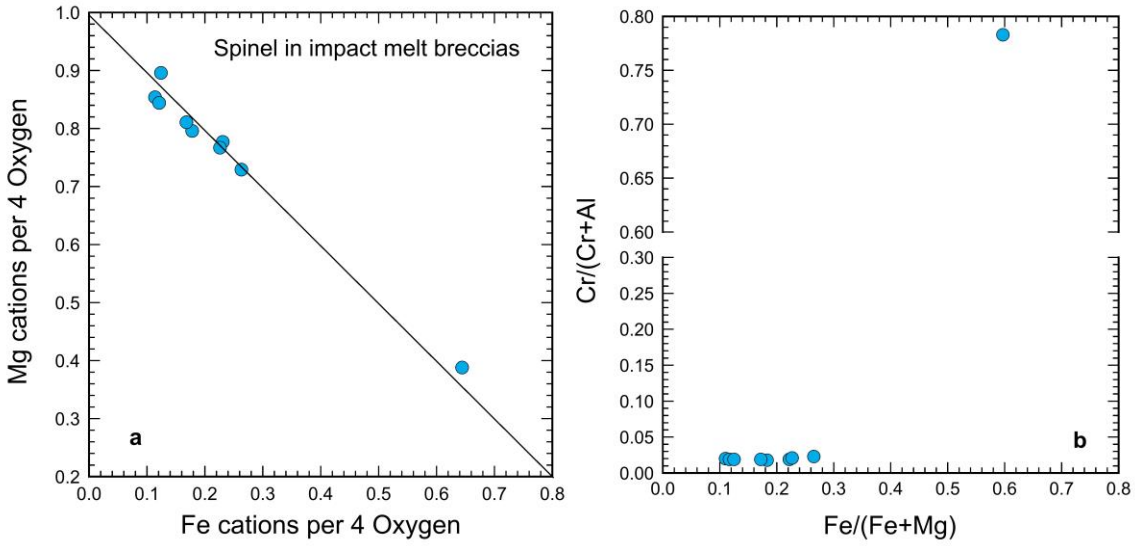

Figure 8. Compositions of spinel in Luna 20 impact melt breccias. (a) Mg vs. Fe cations per formula unit. Line of slope –1 is shown for reference. (b) Atomic Cr/(Cr +Al) vs. Fe/(Fe + Mg).

given in Table 5, including the Cr-Fe spinel and its Mg-Al overgrowth (Fig. 4), which occurs in an impact melt breccia.

Results of an electron probe traverse across this assemblage are illustrated in Fig. 9. The traverse shows that the overgrowth has a uniform composition, and it contrasts sharply with the composition of the core grain, although the overgrowth does have significant Cr (~5 wt% Cr_2O_3) and Fe (~7.5 wt% FeO) components. This chemical sequence is unlike the spinel crystallization sequence observed in many mare basalts; spinels in mare basalt consist mostly of early-formed chromite varieties and late-crystallizing ulvöspinel (Haggerty, 1978).

As reviewed by Papike et al. (1976), workers had interpreted an apparent compositional gap between titanian chromite and chromian ulvöspinel in some Apollo 12 mare basalts as an immiscibility effect. Alternatively, this gap (or compositional bimodality) has also been interpreted as a result of a possible peritectic reaction causing partial resorption of titanian chromite in cases where cooling was moderately slow (e.g., El Goresy et al., 1971; Busche et al., 1972; Papike et al., 1976). The gap may also be crystallo-chemically controlled insofar as intermediate occupation would require a mixture, possibly in domains, of normal and inverse spinels (Haggerty, 2016).

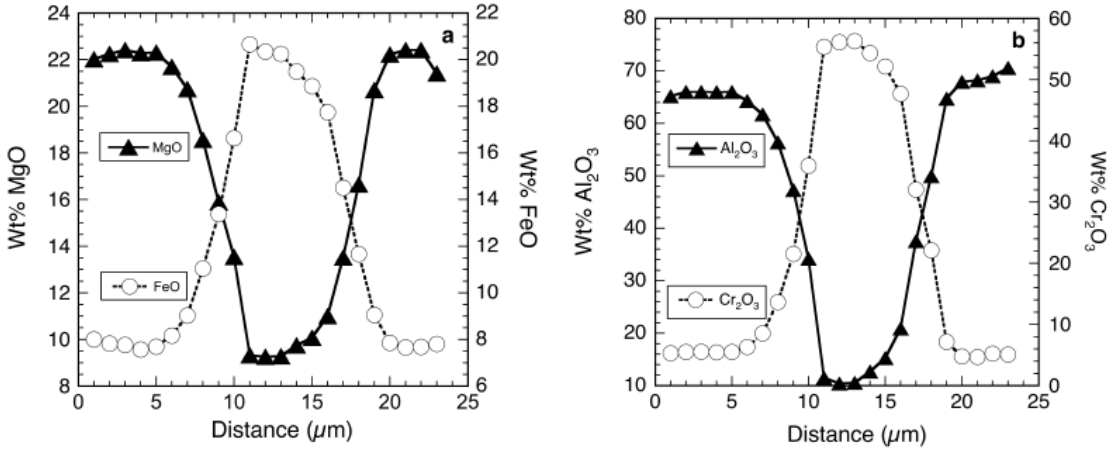

Figure 9. Results of an electron microprobe traverse across the Cr-Fe spinel with Mg-Al spinel overgrowth assemblage shown in Fig. 4c, showing the clear Mg-Fe (a) and Al-Cr (b) composition contrasts.

4. DISCUSSION

4.1. Summary of important petrographic observations of spinel-bearing magmatic lithologies

There is a variety of petrographic and geochemical characteristics that are important in deciphering the origin(s) of these spinel-bearing lithologies.

(1) Based on the Mg# of the mafic silicates and the anorthite contents of the plagioclase, these spinel-bearing lithologies are members of the Mg-suite (Shearer et al., 2021).

(2) The mafic grains are typically less than 50 μm in size and the plagioclase is smaller than 200 μm. This suggests crystallization at a rate faster than some of the deeper troctolites identified at the Apollo 17 site (Shearer et al., 2021).

(3) Olivine occurs as anhedral (no well-formed crystal faces or hexagonal cross-section shapes seen in thin section), equant crystals with no reaction rims of low-Ca

pyroxene. Pyroxene crystallization follows that of olivine and it is not in equilibrium with olivine. This suggests that olivine may have been partially resorbed by the melt, but not through a peritectic reaction such as Olivine + Melt = Orthopyroxene.

(4) Almost all spinel is enclosed in plagioclase. Further, the Mg-Al spinel appears to not be in equilibrium with pyroxene (Figs. 2b-d). This suggests that crystallization took place in the shallow crust and not in the deep crust or mantle (Walker et al., 1972, 1973, 1975; Presnall et al., 1978; Gross & Treiman, 2011).

(5) Pyroxene is subordinate to olivine and is mostly high-Ca pyroxene; low-Ca pyroxene is much less abundant. Neither show exsolution lamellae at a scale of greater than 1μm (Ghose et al., 1973). The submicroscopic nature of the exsolution lamellae indicates that the spinel-bearing rocks crystallized relatively quickly in a shallow (2-3km) crustal environment (Ghose et al., 1973; McCallum & O'Brien, 1996; McCallum & Schwartz, 2001; Shearer & Papike, 2005; McCallum et al., 2006, Shearer et al., 2015; Marks et al., 2019).

4.2. Summary of important petrographic observations of impact-produced lithologies

(1) Significant portions of these samples have a feathery, fine-grained texture (less than 20 μm) consisting of intergrowths of pyroxene and plagioclase. This is suggestive of rather rapid cooling of a melt in the shallow lunar crust (e.g., 1-2 km).

(2) There is significant variation in the composition of larger mineral grains (e.g., olivine, spinel) that have reaction rims or surfaces that provided nucleation sites for subsequent crystals (e.g., Fig. 4). In this particular case, these larger, heterogeneous crystals are relict crystals derived from the original target that have reacted with the impact melt. Therefore, some geochemical features of the target were preserved. Based on the compositions of the relict olivine and plagioclase it is likely that the target was anorthositic troctolite. It would be anticipated that most determinations of the age of this impact melt breccia would yield the age of the impact event.

(3) Many samples have multiple generations of olivine and plagioclase. More Mg-rich olivine is observed to be large and anhedral, whereas smaller, euhedral (well-

formed, with sharp, easily recognized faces), and zoned Fe-rich olivine is closely associated with spinel. Relict plagioclase clasts are anhedral to subhedral, whereas finer-grained plagioclase occurs as abundant laths with interstitial Fe-rich, calcic pyroxene, and as elongate crystals radiating from mineral surfaces (e.g., Fig. 4b). Our preferred interpretation of these textures is that the impact melt was saturated with olivine and spinel and perhaps super-saturated with plagioclase.

(4) There are multiple generations of spinel: subhedral (crystal faces and symmetry partially preserved) and anhedral, Cr-rich spinel that appears to be a relic from the target rock; euhedral to subhedral Mg-Al-spinel rims on Cr-rich spinel; small, euhedral Mg-Al spinel (10-20μm) with thin Fe-enriched rims (1μm). The interpretation of these textures is that the impact melts have the appropriate composition to crystallize Mg-Al spinel in upper crust pressure regimes.

(5) Pyroxenes appear to be in equilibrium with the Mg-Al spinel in some of the samples. Whereas in the discussion of the spinel-bearing magmatic rocks this was implied to be an indication of high-pressure crystallization, such is not the case here, as the pyroxene is both calcic and Fe-rich and therefore the high-pressure equilibria explored by Walker et al. (1972, 1973, 1975) and Presnall et al. (1978) are not relevant to these impact lithologies.

4.3. Origin of the spinel-bearing magmatic lithologies

Gross and Treiman (2011) and Prissel et al. (2014) outlined possible origins for lunar lithologies that contain high modal amounts (up to 30%) of Mg-Al spinel (e.g., ALH81005; pink-spinel anorthosites). Although the spinel-bearing assemblages identified in the Luna 20 samples have only trace abundances of Mg-Al-spinel, similar petrogenetic models are still relevant. There are four hypotheses for the petrogenesis of spinel-bearing lithologies on the Moon: (1) cumulates or restites formed from basaltic systems at high-pressure (Prinz et al., 1973; Anderson, 1973; Bence et al., 1974; Baker & Herzberg, 1980; Marvin et al., 1989; Snyder et al., 1998; Cohen et al., 2001; Takeda et al., 2006); (2) troctolitic melts at low-pressure (Walker et al., 1973; Marvin and Walker, 1985); (3) hybridization of a mantle source or mantle-derived magma (assimilation or cumulate

mixing) (Morgan et al., 2006; Gross & Treiman, 2011; Prissel et al., 2014; Shearer et al., 2015; Elardo et al., 2017, 2020; Treiman et al., 2019); and (4) an exogenic origin, either through a meteoritic component or due to an impact event (Pieters et al., 2011). The latter hypothesis will be considered in discussions of spinel-bearing impact melts.

Walker et al. (1972, 1973), Presnall et al. (1978), Gross and Treiman (2011), and Prissel et al. (2014) showed that at high pressure, the Mg-Al spinel stability field expands and the topology of phase relations changes to enable olivine-saturated, mantle-derived magmas to eventually crystallize spinel + low-Ca pyroxene. This high-pressure origin is probably relevant to some of the spinel- and spinel+cordierite ($(Mg,Fe)_2Al_4Si_5O_{18}$)-bearing assemblages identified in lunar breccias by Dymek et al. (1976) and Baker and Herzberg (1980) (e.g., 72435, 15445). However, textures and mineralogy of the spinel-bearing lithologies returned from the Luna 20 landing site indicate that they are not products of crystallization at high pressure. The spinel-bearing troctolites are relatively fine-grained, suggestive of low pressure and relatively rapid cooling. All pyroxene exsolution lamellae in the Mg-suite lithologies from Luna 20 are sub-microscopic, also implying rapid cooling (e.g., Grove, 1982), and potential depths of origin of 2-4 km (Ghose et al., 1973; Shearer et al., 2021). The interpretation of high- and low-pressure morphologies of the ternary system Olivine-SiO_2-Plagioclase (Walker et al., 1972, 1973; Presnall et al., 1978) led Gross and Treiman (2011) to conclude that low-Ca-pyroxene + spinel should be a common equilibrium assemblage in high-pressure spinel-bearing assemblages. Such assemblages were not identified in the spinel troctolites from Luna 20, however. Finally, modeling of the Crisium impact event indicates that the material excavated to the outer portions of its ejecta blanket may have had relatively shallow origins (Shearer et al., 2021).

As these spinel-bearing magmatic lithologies are products of low-pressure crystallization, what criteria must be met to produce mantle-derived magmas that crystallize spinel-bearing troctolitic cumulates? Within the Olivine-SiO_2-Plagioclase ternary system there are numerous bulk melt compositions that would crystallize Mg-Al spinel (Gross & Treiman, 2011). However, there is a far more limited field of bulk compositions that have olivine as a liquidus phase, as would be expected from a mantle-derived magma, and can still crystallize Mg-Al spinel (e.g., Anorthite side of the tie-line between olivine and spinel + melt $\Rightarrow$ olivine + anorthite peritectic reaction point). Still,

this olivine-saturated melt composition and more Al_2O_3-enriched compositions have the drawback of requiring mantle sources with much higher Al_2O_3/MgO than predicted for lunar mantle compositions produced by all lunar magma ocean crystallization models (S. Taylor & Jakes, 1974; Longhi, 1978; Warren, 1985; S. Taylor et al., 2006; Shearer et al., 2006; Elardo et al., 2011; Elkins-Tanton et al., 2011; Lin et al., 2017). Resorption textures of the spinel could reflect the peritectic reaction spinel + melt $\Rightarrow$ olivine +anorthite, but resorption features of the olivine (without any pyroxene rim) do not appear to reflect this petrogenetic scenario.

As noted above, a major issue with the petrogenesis of mantle-derived magmas capable of crystallizing Mg-Al spinel (in low to very high modal abundances) in relatively shallow crustal environments is that the lunar magma ocean (LMO) cumulate sources have sub-chondritic Al_2O_3/MgO. This is principally the result of plagioclase being sequestered in the uppermost lunar crust during LMO crystallization. A final hypothesis involves the role of plagioclase in either the hybridization of the source for the Mg-suite as a whole, and the spinel troctolites in particular (Shearer et al., 2005, 2015; Elardo et al., 2017, 2020) and the assimilation of plagioclase by mantle-derived, olivine-saturated magmas (Shearer et al., 2005; Gross & Treiman, 2011; Prissel et al., 2014; Treiman et al., 2019).

To produce Mg-suite magmas in a planetary body with a sub-chondritic (Al_2O_3/MgO) mantle, Elardo et al. (2017, 2020) suggested melting of a hybrid cumulate package consisting of deep mantle dunite, crustal anorthosite, and KREEP at the base of the crust under the Procellarum KREEP Terrane (PKT). In this model, these three LMO cumulate components are brought into proximity by overturn resulting from the unstable density and thermal structure of the cumulate pile. Early and deep dunite LMO cumulates with an Mg# of ~90 rose to the base of the ferroan anorthosite lunar crust due to their buoyancy relative to colder, later, and denser Fe-, Ti-rich cumulates. This produces a potential high Al_2O_3/MgO source. As a result of the increased temperature at the base of the lunar crust generated by the hot, early cumulates and the heat-producing elements associated with KREEP, this hybridized source rock melted to form Mg-suite magmas saturated in Mg-rich olivine and calcic plagioclase that have a substantial KREEP component. How does this model fit observations made for the spinel-bearing magmatic lithologies?

Within this dunite-anorthosite hybrid source near the crust-mantle interface, melting would have occurred at the olivine-pyroxene-spinel peritectic or the plagioclase-pyroxene-spinel peritectic within the Olivine-Anorthite-Silica ternary. The peritectic where melting would occur is dependent upon the proportions of dunite and anorthosite. Still, these melts would have compositions with relatively high, super-chondritic Al_2O_3/MgO. Once these melts were transported to the upper lunar crust environment, however, the melts would no longer have been in the spinel field. At low pressures these melts would crystallize olivine + plagioclase. Although the crystallization products of these melt compositions would be analogous to most Mg-suite rocks, spinel would not be in the assemblage, and this does not fit our textural observations. Further, olivine in the spinel troctolites from Luna 20 has resorption features which cannot be accounted for by crystallization in the olivine field, along the plagioclase-olivine cotectic, or at the Olivine + Low-Ca pyroxene + plagioclase peritectic. The expected olivine texture was most likely produced by the reaction Olivine + Melt $\Rightarrow$ Low-Ca pyroxene + plagioclase.

The hybrid source model was investigated experimentally by Prissel et al. (2016). They found that such Al_2O_3-rich melts yielded Mg-Al spinel, and thus the model could account for the origin of pink-spinel troctolites, which are very rare, but not Cr-spinel-bearing troctolite. The experimental results of Prissel et al. (2016) do not support a hybridized source such as that described above for most spinel troctolites.

In addition, a Mg-suite model that requires an upper mantle dominated by olivine is not consistent with remote sensing observations or dynamical models of gravitational restructuring. Specifically, mantle materials ejected and melted during the South Pole-Aitken basin-forming event appear to be dominated by pyroxene + ilmenite- and KREEP-bearing cumulates (Nakamura et al., 2009; Moriarty et al., 2013, 2021a,b; Moriarty & Pieters, 2018). The impact melt associated with the Crisium basin is dominated by low-Ca pyroxene (Runyon et al., 2020). Generation of an olivine-poor, pyroxene-rich upper mantle has been modeled by Prissel and Gross (2020). Dynamical models of LMO evolution also suggest that mafic mantle cumulates (olivine and pyroxene) become well-mixed during gravitational restructuring (Boukaré et al. 2018), while a significant fraction (~30%) of late-stage ferroan cumulates (enriched in KREEP and Ti) are stable in the uppermost mantle over geologic time (Zhao et al., 2019).

A final scenario for generating spinel-bearing magmatic assemblages, which differs from models that produce typical Mg-suite members, is assimilation of ferroan anorthosite crust by primitive, Mg-rich, mantle-derived magmas (Finnila et al., 1994; Shearer et al., 2005; Morgan et al., 2006; Gross & Treiman, 2011; Prissel et al., 2014; Treiman et al., 2019). This has been demonstrated to be a favorable process to account for observations of magmatic rocks with high spinel contents (e.g., pink-spinel anorthosites, ALHA 81005), but is it appropriate for these shallow spinel troctolites? Gross and Treiman (2011), Prissel et al. (2014), and Treiman et al. (2019) demonstrated in the Forsterite-Anorthosite-SiO_2 ternary and Forsterite-Anorthite binary systems that assimilation of anorthositic wall rock by an olivine-saturated melt could produce melts in the spinel stability field. These melts would have a crystallization sequence of spinel $\Rightarrow$ spinel + plagioclase $\Rightarrow$ spinel + melt react to plagioclase + olivine $\Rightarrow$ plagioclase + olivine $\Rightarrow$ olivine + melt reacts to plagioclase + low-Ca pyroxene. This appears to be the approximate fractional crystallization sequence typically observed in the spinel troctolites. Although we found high-Ca pyroxene in spinel troctolites in the present suite (Table 1), we found low-Ca pyroxene in anorthositic troctolites, and Prinz et al. (1973) found no high-Ca pyroxene in the Luna 20 troctolites they studied but reported a range of 0 – 8% normative hypersthene for spinel troctolite. Gross and Treiman (2011) suggested that such a process would displace previously crystallized olivine off of the liquidus, resulting in the resorption features observed in the olivine in the troctolite. Addition of a ferroan component could account for the relatively Fe-rich quench olivines found in the impact melt rock shown in Fig. 4.

There are shortcomings of this model, including requiring a very specific geometry among mixed components, temperature of components and phase relationships. The model also assumes that primitive, Mg-rich, mantle-derived magmas are one component. However, this petrogenetic hypothesis is the best fit thus far to our observations, and it appears to be consistent with the constraints from remote sensing mentioned above.

4.4. Origin of the spinel-bearing impact melt lithologies

The models discussed above, however, are not relevant to impact-produced melt assemblages. Pieters et al. (2011) suggested an exogenic origin for some of the spinel-

bearing lunar lithologies, either through addition of a meteoritic component or due to an impact event. Our observations suggest an exogenic origin may be appropriate for some of the spinel lithologies, but a meteoritic component is not necessary. The stability of Mg-Al spinel in these low-pressure, relatively quickly cooled melt systems provides some insights into the role of the plagioclase component in the petrogenesis of Mg-Al spinel in both magmatic and impact-produced lithologies. The impact melt breccia shown in Figure 4 perhaps illustrates this the best. The relict mineralogy in the breccia, plagioclase (An_{94-96}), olivine (Fo_{79-89}), and Cr-Fe spinel (56 wt% Cr_2O_3, 23 wt% FeO) is representative of a troctolitic anorthosite (i.e., an Mg-suite sample). The impact melt component crystallized to an assemblage of fine plagioclase laths (An_{93-95}), with interstitial olivine (Fo_{82}) and pyroxene ($En_{64}Wo_6Fs_{30}$), with accessory Mg-Al-dominated spinel and local, euhedral, relatively Fe-rich (Fo_{71-82}, Fig. 4c) olivine. The crystallization sequence appears to be plagioclase (radiating from relict mineral grains) $\Rightarrow$ olivine and spinel $\Rightarrow$ fine grained intergrowth of pyroxene and plagioclase. If the plagioclase radiating from the surface of relict olivine is analogous to that in mare basalts such as Apollo 15 quartz-normative basalts (e.g., 15499), these textures could represent rapid cooling (10°C/hour) of a plagioclase-oversaturated melt (Bence & Papike, 1972; Grove & Walker, 1977; Shearer et al., 1989).

Within the low-pressure Forsterite-Anorthite-SiO_2 system, the bulk composition of this sample is within the plagioclase stability field. Under equilibrium conditions, after plagioclase crystallization, the melt composition would move along the plagioclase-spinel cotectic. This would drive the melt to the plagioclase-spinel-olivine peritectic, where the spinel would be consumed through the reaction spinel + liquid $\Rightarrow$ plagioclase + olivine. The textures in Figure 4 do not reflect this reaction; both spinel and olivine are euhedral and appear to be stable. An interpretation is that disequilibrium crystallization of plagioclase drove the melt composition across the spinel field to the olivine-spinel cotectic. Rapid fractional crystallization drove the melt to co-precipitation of plagioclase and Fe-rich pyroxene. The melt pockets in the breccia are small and contain a relatively high percentage of Mg-Al spinel.

4.5. Value of robotically collected samples

691

692 The automated Luna 20 mission returned a soil core with a mass of ~50 g, of which
693 NASA was allocated 2.04 g. This is much less material than the yields of any of the Apollo
694 returns, but, as the present study and numerous others show, much can be learned from it.
695 In addition to details of local igneous lithologies, fragments of impact melt rocks in the
696 sample can provide valuable information about basin-forming impacts, such as: the nature
697 of the target rocks; the nature, original depth, and distribution of excavated material; and
698 the age of the event. In addition, the Luna 20 sample provides materials necessary for
699 calibration and improved interpretation of remotely sensed data used for identification of
700 lithologies distributed about the region. From micron-scale observations and analyses to
701 improved understanding of regional geology and major events in the history of the Moon,
702 much information can be extracted from a small regolith sample collected from a known
703 location. Robotically collected samples can be an important complement to extensive
704 sampling and exploration of a site by astronauts.

705

706 ## 5. CONCLUSIONS

707

708 Although the spinel-bearing lithologies sampled at the Luna 20 site do not have
709 modal mineralogies similar to either the hypothesized "pink-spinel" anorthosites" or
710 recently documented spinel-rich lunar meteorites, their existence in the highlands adjacent
711 to the Crisium basin sheds light on the origin of lunar highlands lithologies in general, and
712 the spinel-bearing assemblages in particular. We further conclude:

713 (1) Mg-Al spinel-bearing assemblages in lunar rocks are products of both magmatic
714 and impact processes.
715 (2) The Luna 20 spinel-bearing magmatic lithologies are members of the Mg-suite.
716 (3) The spinel in these magmatic assemblages crystallized in a relatively shallow
717 crustal environment.
718 (4) Although there are numerous possible models for the petrogenesis of spinel-bearing
719 magmatic assemblages, the assimilation of plagioclase-rich crust by a mantle-
720 derived, olivine-saturated magma remains the best way to accommodate sample-

based and remotely sensed observations. Mixing proportions of melt and plagioclase may result in high proportions of plagioclase and spinel.

(5) Impact processes can produce spinel-bearing feldspathic assemblages. Depending on the degree of equilibrium and crustal target composition, it is possible to produce lithologies with high abundances of plagioclase and spinel. It is likely that the corresponding target rock would be anorthositic troctolite (Mg-suite).

(6) Finally, this study and others illustrate that even a few fragments from a relatively small robotically collected core sample from a single location provides insights into a diverse array of lunar petrologic processes.

ACKNOWLEDGMENTS

Thorough and helpful reviews were provided by Drs. S. Elardo and T. Prissel, and their efforts are appreciated. M. Spilde assisted with electron probe analysis. This work was supported by NASA through LDAP grant # 80NSSC19K1099 to CKS and NP. DPM is further supported by NASA under award number 80GSFC21M0002.

Data availability statement

The data collected by the authors for this work (backscattered electron images and quantitative analyses) are publicly available from the open access institutional repository of the University of New Mexico, https://digitalrepository.unm.edu/eps_fsp/14. Literature data (spinel analyses) plotted in Fig. 6 are from Haggerty (1973), Brett et al. (1973), Cameron et al. (1973), G. Taylor et al. (1973), Prinz et al. (1973), and Meyer (1973).

REFERENCES

Anderson, A. T. (1973). The texture and mineralogy of lunar peridotite, 15445,10. *Journal of Geology, 81*, 219-226. https://doi.org/10/1086/626837

754 Antonini, A. S., Ganuza, M. L., Ferracutti, G., Gargiulo, M. F., Matkovic, K., Gröller, E.,
755 et al. (2020). Spinel web: an interactive web application for visualizing the
756 chemical composition of spinel group minerals. *Earth Science Informatics*,
757 https://doi.org/10.1007/s12145-020-00542-w
758
759 Baker, M. & Herzberg, C. (1980). Spinel cataclasites in 15445 and 72435: Petrology and
760 criteria for equilibrium. *Proceedings of the 11th Lunar and Planetary Science*
761 *Conference*, 535-553.
762
763 Bence, A. E., Delano, J. W., Papike, J. J., & Cameron, K. L. (1974). Petrology of the
764 highlands massifs at Taurus-Littrow: An analysis of the 2–4 mm soil fraction. In
765 *Proceedings of the 5th Lunar Science Conference* (pp. 785-827). New York, NY:
766 Pergamon Press.
767
768 Bence, A. E., & Grove, T. L. (1978). The Luna 24 highland component. In R. B. Merrill &
769 J. J. Papike (Eds.), *Mare Crisium: The View from Luna 24* (pp. 429-444). New
770 York, NY: Pergamon Press.
771
772 Bence, A. E., & Papike, J. J. (1972). Pyroxenes as recorders of lunar basalt petrogenesis:
773 Chemical trends due to crystal-liquid interaction. In *Proceedings of the 3rd Lunar*
774 *Science Conference* (pp. 431-469). New York, NY: Pergamon Press.
775
776 Boukaré, C. E., Parmentier, E. M., & Parman, S. W. (2018). Timing of mantle overturn
777 during magma ocean solidification. *Earth and Planetary Science Letters, 491*, 216-
778 225.
779
780 Brett R., Gooley R. C., Dowty E., Prinz M., & Keil K. (1973). Oxide minerals in lithic
781 fragments from Luna 20 fines. *Geochimica et Cosmochimica Acta,37,* 761-773.
782
783 Busche, F. D., Prinz, M., Keil, K., & Bunch, T. E. (1972). Spinels and the petrogenesis of
784 some Apollo 12 igneous rocks. *American Mineralogist, 57*(11-12), 1729-1747.

Cameron K. L., Papike J. J., Bence A. E., & Sueno S. (1973). Petrology of fine-grained rock fragments and petrologic implications of single crystals from the Luna 20 soil. *Geochimica et Cosmochimica Acta, 37,* 775-793.

Cohen, B. A., Snyder, G. A., Hall, C. M., Taylor, L. A., & Nazarov, M. A. (2001). Argon-40-argon-39 chronology and petrogenesis along the eastern limb of the Moon from Luna 16, 20 and 24 samples. *Meteoritics & Planetary Science, 36,* 1345-1366.

Conrad, G. H., Hlava P. F., Green, J. R., Moore, R. B., Moreland, G., Dowty, E., et al. (1973). Electron microprobe analyses of lithic fragments and their minerals from Luna 20 fines. *Special Publication Number 12*, Albuquerque, NM, UNM Institute of Meteoritics. 62pp.

Corley, L. M., McGovern, P. J., Kramer, G. Y., Lemelin, M., Trang, D., Gillis-Davis, J. J., et al. (2018). Olivine-bearing lithologies on the Moon: constraints on origins and transport mechanisms from M3 spectroscopy, radiative transfer modeling, and GRAIL crustal thickness. *Icarus, 300,* 287-304.

Dhingra, D., Pieters, C. M., Boardman, J. W., Head, J. W., Isaacson, P. J., & Taylor, L. A. (2011). Compositional diversity at Theophilus Crater: Understanding the geological context of Mg-spinel bearing central peaks. *Geophysical Research Letters, 38*, L11201, doi:10.1029/2011GL047314.

Dymek, R. F., Albee, A. L., & Chodos, A. A. (1976). Petrology and origin of Boulders no. 2 and no. 3, Apollo 17 Station 2. In *Proceedings of the 7th Lunar Science Conference* (pp. 2335-2378). New York, NY: Pergamon Press.

Elardo, S. M., Draper, D. S., & Shearer Jr., C. K. (2011). Lunar magma ocean crystallization revisited: Bulk composition, early cumulate mineralogy, and the

source regions of the highlands Mg-suite. *Geochimica et Cosmochimica Acta*, *75*(11), 3024-3045.

Elardo, S. M., Laneuville, M., McCubbin, F. M., & Shearer, C. K. (2020). Early crust building enhanced on the Moon's nearside by mantle melting-point depression. *Nature Geoscience*, *13*(5), 339-343.

Elardo, S. M., Shearer, C. K., & McCubbin, F. M. (2017). *The role of KREEP in the production of Mg-suite magmas and its influence on the extent of Mg-suite magmatism in the lunar crust*. Paper presented at 48th Lunar Planetary Science Conference (abstract #2450), Lunar and Planetary Institute, The Woodlands, TX.

El Goresy, A., Ramdohr, P., & Taylor, L. A. (1971). The geochemistry of the opaque minerals in Apollo 14 crystalline rocks. *Earth and Planetary Science Letters*, *13*(1), 121-129.

Elkins-Tanton, L. T., Burgess, S., & Yin, Q. Z. (2011). The lunar magma ocean: Reconciling the solidification process with lunar petrology and geochronology. *Earth and Planetary Science Letters*, *304*(3-4), 326-336.

Finnila, A. B., Hess, P. C., & Rutherford, M. J. (1994). Assimilation by lunar mare basalts: Melting of crustal material and dissolution of anorthite. *Journal of Geophysical Research: Planets*, *99*(E7), 14677-14690.

Ghose, S., McCallum, I. S., & Tidy, E. (1973). Luna 20 pyroxenes: exsolution and phase transformation as indicators of petrologic history. *Geochimica et Cosmochimica Acta*, *37*(4), 831-839.

Gross, J., Gillis-Davis, J., Isaacson, P. J., & Le, L. (2015). *How rich is rich? Placing constraints on the abundance of spinel in the pink spinel anorthosite lithology on the Moon through space weathering.* Paper presented at 46th Lunar and Planetary

Science Conference (Abstract #2642), Lunar and Planetary Institute, The Woodlands, TX.

Gross J., & Treiman A. H. (2011). Unique spinel-rich lithology in lunar meteorite ALHA 81005: Origin and possible connection to M3 observations of the farside highlands. *Journal of Geophysical Research, 116,* E10009, doi: 10.1029/2011JE003858.

Grove, T. L. (1982). Use of exsolution lamellae in lunar clinopyroxenes as cooling rate speedometers: an experimental calibration. *American Mineralogist, 67,* 251-268.

Grove, T. L. & Walker, D. (1977). Cooling histories of Apollo 15 quartz-normative basalts. In *Proceedings of the 8th Lunar Science Conference* (pp. 1501-1520). New York, NY: Pergamon Press.

Haggerty, S. E. (1972). Luna 16: an opaque mineral study and a systematic examination of compositional variations of spinels from Mare Fecunditatis. *Earth and Planetary Science Letters, 13,* 328-352.

Haggerty, S. E. (1973). Luna 20: mineral chemistry of spinel, pleonaste, chromite, ulvöspinel, ilmenite and rutile. *Geochimica et Cosmochimica Acta, 37,* 857-867.

Haggerty, S. E. (2016). Spinels in planetary systems. *American Mineralogist, 101,* 5-6.

Haggerty, S. E. (1978). Luna 24: Systematics in spinel mineral chemistry in the context of an intrusive petrogenetic grid. In J. J. Papike & R. B. Merrill (Eds.), *Mare Crisium: The View from Luna 24* (pp. 523-535). New York, NY: Pergamon Press.

Herzberg, C. T. (1978). The bearing of spinel cataclasites on the crust-mantle structure of the moon. In *Proceedings of the 9th Lunar and Planetary Science Conference* (pp. 319-336). New York, NY: Pergamon Press.

877 Herzberg, C. T. & Baker, M. B. (1980). The cordierite- to spinel-cataclasite transition:
878 Structure of the lunar crust. In J. J. Papike & R. B. Merrill (Eds.), *Proceedings of*
879 *the Conference on the Lunar Highlands Crust* (pp. 113-132). New York, NY:
880 Pergamon Press.
881
882 Lemelin, M., Lucey, P. G., Miljković, K., Gaddis, L. R., Hare, T., & Ohtake, M. (2019).
883 The compositions of the lunar crust and upper mantle: Spectral analysis of the inner
884 rings of lunar impact basins. *Planetary and Space Science, 165*, 230-243.
885
886 Lin, Y., Tronche, E. J., Steenstra, E. S., & van Westrenen, W. (2017). Evidence for an early
887 wet Moon from experimental crystallization of the lunar magma ocean. *Nature*
888 *Geoscience, 10*, 14-18.
889
890 Longhi, J. (1978). Pyroxene stability and the composition of the lunar magma ocean. In
891 *Proceedings of the 9th Lunar and Planetary Science Conference*, (pp. 285-306).
892 New York, NY: Pergamon Press.
893
894 Marks, N. E., Borg, L. E., Shearer, C. K., & Cassata, W. S. (2019). Geochronology of an
895 Apollo 16 clast provides evidence for a basin-forming impact 4.3 billion years
896 ago. *Journal of Geophysical Research: Planets, 124*, 2465-2481.
897
898 Marvin, U. B. & Walker, D. (1985). A transient heating event in the history of a highlands
899 troctolite from Apollo 12 soil 12033. *Journal of Geophysical Research: Solid*
900 *Earth*, 90 (S02), C421-C429.
901
902 Marvin, U. B., Carey, J. W. & Lindstrom, M. M. (1989). Cordierite-spinel troctolite, a new
903 magnesium-rich lithology from the lunar Highlands. *Science, 243*, 925-928.
904
905 McCallum, I. S., Domeneghetti, M. C., Schwartz, J. M., Mullen, E. K., Zema, M., Camara,
906 F., et al. (2006). Cooling history of lunar Mg-suite gabbronorite 76255 troctolite

76535 and Stillwater pyroxenite SC-936: The record in exsolution and ordering in pyroxene. *Geochimica et Cosmochimica Acta*, *70,* 6068-6078.

McCallum, I. S., & O'Brien, H. E. (1996). Stratigraphy of the lunar highland crust: Depths of burial of lunar samples from cooling-rate studies. *American Mineralogist, 81*, 1166-1175.

McCallum I. S., & Schwartz, J. M. (2001). Lunar Mg suite: Thermobarometry and petrogenesis of parental magmas. *Journal of Geophysical Research, 106*, 27969-27984.

Meyer, H. O. A. (1973). Luna 20: Mineralogy and petrology of fragments less than 125µm size. *Geochimica et Cosmochimica Acta, 37,* 943-952.

Miljković, K., Wieczorek, M. A., Collins, G. S., Solomon, S. C., Smith, D. E., & Zuber, M. T. (2015). Excavation of the lunar mantle by basin-forming impact events on the Moon. *Earth and Planetary Science Letters, 409*, 243-251.

Morgan, Z., Liang, Y., & Hess, P. (2006). An experimental study of anorthosite dissolution in lunar picritic magmas: implications for crustal assimilation processes. *Geochimica et Cosmochimica Acta, 70*, 3477-3491.

Moriarty III, D. P., Dygert, N., Valencia, S. N., Watkins, R. N., & Petro, N. E. (2021a). The search for lunar mantle rocks exposed on the surface of the Moon. *Nature Communications, 12*, 4659. https://doi.org/10.1038/s41467-021-24626-3.

Moriarty III, D. P., & Pieters, C. M. (2018). The character of South Pole-Aitken Basin: Patterns of surface and subsurface composition. *Journal of Geophysical Research: Planets*, *123*(3), 729-747.

Moriarty III, D. P., Pieters, C. M., & Isaacson, P. J. (2013). Compositional heterogeneity of central peaks within the South Pole-Aitken Basin. *Journal of Geophysical Research: Planets,* 118, 2310-2322.

Moriarty III, D. P., Simon, S. B., Shearer, C. K., Haggerty, S. E., Petro N., & Li, S. (2022). *Orbital assessment of the distribution and composition of spinel across the Crisium region: Insights from Luna 20 samples.* Paper presented at 53rd Lunar and Planetary Science Conference (Abstract #2139, Lunar and Planetary Institute, The Woodlands, TX.

Moriarty III, D. P., Watkins, R. N., Valencia, S. N., Kendall, J. D., Evans, A. J., Dygert, N., & Petro, N. E. (2021b). Evidence for a Stratified Upper Mantle Preserved within the South Pole–Aitken Basin. *Journal of Geophysical Research: Planets*, e2020JE006589.

Nakamura, R., Matsunaga, T., Ogawa, Y., Yamamoto, S., Hiroi, T., Saiki, K., et al. (2009). Ultramafic impact melt sheet beneath the South Pole–Aitken basin on the Moon. *Geophysical Research Letters*, *36*(22). doi:10.1029/2009GL040765

Neumann, G. A., Zuber, M. T., Wieczorek, M. A., Head, J. W., Baker, D. M., Solomon, S. C., et al. (2015). Lunar impact basins revealed by Gravity Recovery and Interior Laboratory measurements. *Science Advances*, *1*(9), e1500852.

Papike, J. J., Hodges, F. N., Bence, A. E., Cameron, M., & Rhodes, J. M. (1976). Mare basalts: Crystal chemistry, mineralogy, and petrology. *Reviews of Geophysics, 14*, 475-540.

Pieters, C. M., Besse, S., Boardman, J., Buratti, B., Cheek, L., Clark, R. N., et al. (2011). Mg-spinel lithology: A new rock type on the lunar farside. *Journal of Geophysical Research: Planets*, 116 (E6), https://doi.org/10.1029/2010JE003727

968 Pieters, C. M., Boardman, J., Buratti, B., Chatterjee, A., Clark, R., Glavich, T., et al. (2009).
969 The Moon mineralogy mapper (M³) on Chandrayaan-1. *Current Science, 96(4)*,
970 500-505.
971
972 Pieters, C., Hanna, K. H., Cheek, L., Dhingra, D., Prissel, T., Jackson, C., et al. (2014).
973 The distribution of Mg-spinel across the Moon and constraints on crustal origin.
974 *American Mineralogist*, 99, 1893-1910. https://doi.org/10.2138/am-2014-4776.
975
976 Presnall, D. C., Dixon, S. A., Dixon, J. R., O'Donnell, T. H., Brenner, N. L., Schrock, R.
977 L., & Dycus, D. W. (1978). Liquidus phase relations on the join diopside-forsterite-
978 anorthite from 1 atm to 20 kbar: their bearing on the generation and crystallization
979 of basaltic magma. *Contributions to Mineralogy and Petrology*, 66, 203-220.
980
981 Prinz, M., Dowty, E., Keil, K. & Bunch, T. E. (1973). Mineralogy, petrology and chemistry
982 of lithic fragments from Luna 20 fines: origin of the cumulate ANT suite and its
983 relationship to high-alumina and mare basalts. *Geochimica et Cosmochimica Acta*,
984 37, 979-1006.
985
986 Prissel, T. C., & Gross, J. (2020). On the petrogenesis of lunar troctolites: New insights
987 into cumulate mantle overturn and mantle exposures in impact basins. *Earth and*
988 *Planetary Science Letters*, 551, 116531.
989 https://doi.org/10.1016/j.epsl.2020.116531
990
991 Prissel, T. C., Parman, S. W., & Head, J. W. (2016). Formation of the lunar highlands Mg-
992 suite as told by spinel. *American Mineralogist*, 101, 1624-1635l
993
994 Prissel, T. C., Parman, S. W., Jackson, C. R. M., Rutherford, M. J., Hess, P. C., Head, J.
995 W., et al. (2014). Pink Moon: The petrogenesis of pink spinel anorthosites and
996 implications concerning Mg-suite magmatism. *Earth and Planetary Science*
997 *Letters*, 403, 144-156.
998

Runyon, K. D., Moriarty III, D. P., Denevi, B. W., Greenhagen, B. T., Morgan, G., Young, K. E., et al. (2020). Impact melt facies in the Moon's Crisium basin: Identifying, characterizing, and future radiogenic dating. *Journal of Geophysical Research: Planets 125*, 10.1029/2019JE006024.

Shearer, C. K., Elardo, S. M., Petro, N. E., Borg, L. E., & McCubbin, F. M. (2015). Origin of the lunar highlands Mg-suite: An integrated petrology, geochemistry, chronology, and remote sensing perspective. *American Mineralogist*, 100, 294-325.

Shearer, C. K., Hess, P. C., Wieczorek, M. A., Pritchard, M. E., Parmentier, E. M., Borg, L. E., et al. (2006). Thermal and magmatic evolution of the Moon. *Reviews in Mineralogy and Geochemistry, 60*, 365-518.

Shearer, C. K., Moriarty, D. P., Simon, S. B., Petro, N., & Papike, J. J. (2022). *Where is the lunar mantle and deep crust at Crisium? Placing the Luna 20 samples within the context of the Crisium Basin-forming event.* Paper presented at 53rd Lunar and Planetary Science Conference (Abstract #1647), Lunar and Planetary Institute, The Woodlands, TX.

Shearer, C. K., & Papike, J. J. (2005). Early crustal building processes on the moon: Models for the petrogenesis of the magnesian suite. *Geochimica et Cosmochimica Acta* 69, 3445-3461.

Shearer, C. K., Papike, J. J., Simon, S. B., & Shimizu, N. (1989). An ion microprobe study of the intra-crystalline behavior of REE and selected trace elements in pyroxene from mare basalts with different cooling and crystallization histories. *Geochimica et Cosmochimica Acta* 53, 1041-1054.

Shearer, C. K., Simon, S. B., Petro, N., Moriarty, D., Papike, J. J. & Joyce, F. S. (2021). *The evolution of the lunar crust I. A multi-perspective approach to understanding*

the origin of FAN and Mg-suite lithologies at the Luna 20 landing site. Paper presented at 52nd Lunar and Planetary Science Conference (Abstract #1155), Lunar and Planetary Institute, Virtual.

Simon, S. B., Shearer, C. K., Haggerty, S. E., Papike, J. J., Petro, N., Moriarty, D. & Vaci, Z. (2021). *The evolution of the lunar crust II. A multi-perspective approach to understanding the origin of spinel-bearing lithologies at the Luna 20 landing site.* Paper presented at 52nd Lunar and Planetary Science Conference (Abstract # 1672), Lunar and Planetary Institute, Virtual.

Simon, S. B., Shearer, C. K., Haggerty, S. E., Moriarty, D., Petro, N., Papike, J. J., & Vaci, Z. (2022). *Shallow crustal origins for spinel-bearing lithologies on the Moon: A perspective from the Luna 20 mission*. Paper presented at 53rd Lunar and Planetary Science Conference (Abstract #1623), Lunar and Planetary Institute, The Woodlands, TX.

Sliz, M. & Spudis, P. (2016). *New geological map of the lunar Crisium basin*. Paper presented at 47th Lunar and Planetary Science Conference (Abstract #1678), Lunar and Planetary Institute, The Woodlands, TX.

Snyder, G. A., Ruzicka, A. M., Taylor, L. A. & Patchen, A. D. (1998). *Journey to the center of the regolith: A spinel troctolite and other clasts from drive tube 68001*. Paper presented at 29th Lunar and Planetary Science Conference (Abstract #1144), Lunar and Planetary Institute, Houston, TX.

Snyder, G. A., Taylor, L. A., Patchen, A., Nazarov, M. A. & Semenova, T. S. (1999). Mineralogy *and petrology of a primitive troctolite and gabbros from Luna 20, eastern highlands of the Moon.* Paper presented at 30th Lunar and Planetary Science Conference (Abstract #1491), Lunar and Planetary Institute, Houston, TX.

1060 Stöffler, D., Knöll, H. D., Marvin, U. B., Simonds, C. H., & Warren, P. H. (1980).
1061 Recommended classification and nomenclature of lunar highland rocks - a
1062 committee report. In J. J. Papike and R. B. Merrill (Eds.), *Proceedings of the*
1063 *Conference on the Lunar Highlands Crust* (pp. 51-70). New York, NY: Pergamon
1064 Press.
1065
1066 Sun, Y., Lin, L., & Zhang, Y. (2017). Detection of Mg-spinel bearing central peaks using
1067 M^3 images: Implications for the petrogenesis of Mg-spinel. *Earth and Planetary*
1068 *Science Letters*, 465, 45-68.
1069
1070 Takeda, H., Yamaguchi, A., Bogard, D. D., Karouji, Y., Ebihara, M., Ohtake, M., et al.
1071 (2006). Magnesian anorthosites and a deep crustal rock from the farside crust of the
1072 moon. *Earth and Planetary Science Letters 247 (3-4)*, 171-184.
1073
1074 Taylor, G. J., Drake, M. J., Wood, J. A., & Marvin, U. B. (1973). The Luna 20 lithic
1075 fragments, and the composition and origin of the lunar highlands. *Geochimica et*
1076 *Cosmochimica Acta*, 37, 1087-1106.
1077
1078 Taylor, S. R. & Jakes, P. (1974). The geochemical evolution of the Moon. In *Proceedings*
1079 *of the 5th Lunar Science Conference*, 1287–1305. New York, NY: Pergamon Press.
1080
1081 Taylor, S. R., Taylor, G. J., & Taylor, L. A. (2006). The moon: A Taylor
1082 perspective. *Geochimica et Cosmochimica Acta*, *70*(24), 5904-5918.
1083
1084 Treiman, A. H., Kulis, M. J., & Glazner, A. F. (2019). Spinel-anorthosites on the Moon:
1085 Impact melt origins suggested by enthalpy constraints. *American Mineralogist* 104,
1086 370-384.
1087
1088 Walker, D., Grove, T. L., Longhi, J., Stolper, E. M., & Hays, J. F. (1973). Origin of lunar
1089 feldspathic rocks. *Earth and Planetary Science Letters 20*, 325-336.
1090

Walker, D., Longhi, J., & Hays, J. (1972). Experimental petrology and origin of Fra Mauro rocks and soil. In *Proceedings of the 3rd Lunar Science Conference*, 797-817. Cambridge, MA: The M.I.T. Press.

Walker, D., Longhi, J., & Hays, J. F. (1975). Differentiation of a very thick magma body and implications for the source regions of mare basalts. *Proceedings of the 6th Lunar Science Conference*, 1103-1120. New York, NY: Pergamon Press.

Warren, P. H. (1985). The magma ocean concept and lunar evolution. *Annual Review of Earth and Planetary Sciences* 13, 201-240.

Wieczorek, M. A., Neumann, G. A., Nimmo, F., Kiefer, W. S., Taylor, G. J., Melosh, H. J., et al. (2013). The crust of the Moon as seen by GRAIL. *Science* 339(6120), 671-675.

Yamamoto, S., Nakamura, R., Matsunaga, T., Ogawa, Y., Ishihara, Y., Morota, T., et al. (2010). Possible mantle origin of olivine around lunar impact basins detected by SELENE. *Nature Geoscience*, 3, 533-536.

Zhou, Y., de Vries, J., van den Berg, A. P., Jacobs, M. H. G., & van Westrenen, W. (2019). The participation of ilmenite-bearing cumulates in lunar mantle overturn. *Earth and Planetary Science Letters, 511*, 1-11.

1120